Neural network activity in the neonatal acute slice, slice culture and cell culture

Dissertation

Zur Erlangung des Grades
Doktor der Naturwissenschaften

Am Fachbereich Biologie
Der Johannes Gutenberg-Universität
Mainz

vorgelegt von

Jyh-Jang Sun

geb. am 11.04.1974 in Taiwan

Mainz, 2009

Tag der mündlichen Prüfung: 08.June.2009

“Consciousness is a biological process. “

Eric R. Kandel

Table of contents

Abbreviations

α	Alpha frequency range (8-13 Hz)
β	Beta frequency range (13-30 Hz)
γ	Gamma frequency range (30-80 Hz)
δ	Delta frequency range (0.5-4 Hz)
θ	Theta frequency range (4-7 Hz)
ACh	Acetylcholine
ACSF	Artificial cerebrospinal fluid
ADC	Analogue-to-digital conversion
AMPA	α-amino-3-hydroxy-5-methyl-4-isoxazolepropionic acid
ANOVA	Analysis of variance
AP	Action potential
BI	Burst index
CP	Cortical plate
EPSP	Excitatory postsynaptic potential
GABA	γ-aminobutyric acid
ICPs	Internal cognitive processes
ISI	Inter-spike interval
Hz	Hertz
LFP	Local field potential
MEA	Micro-electrode arrays
MZ	Marginal zone
NMDA	N-methyl-D-aspartic acid
PP	Preplate
REM	Rapid eye movement
SP	Subplate
SVZ	Subventricular zone
VZ	Ventricular zone

List of figures

1. Introduction

The early cortical neuronal networks

During embryonic development, immature neuronal circuits are established on the basis of genetic information. Afterwards, perinatal neuronal activity plays the determining role for tuning the development of neuronal networks (Figure 1) (Khazipov and Luhmann, 2006).

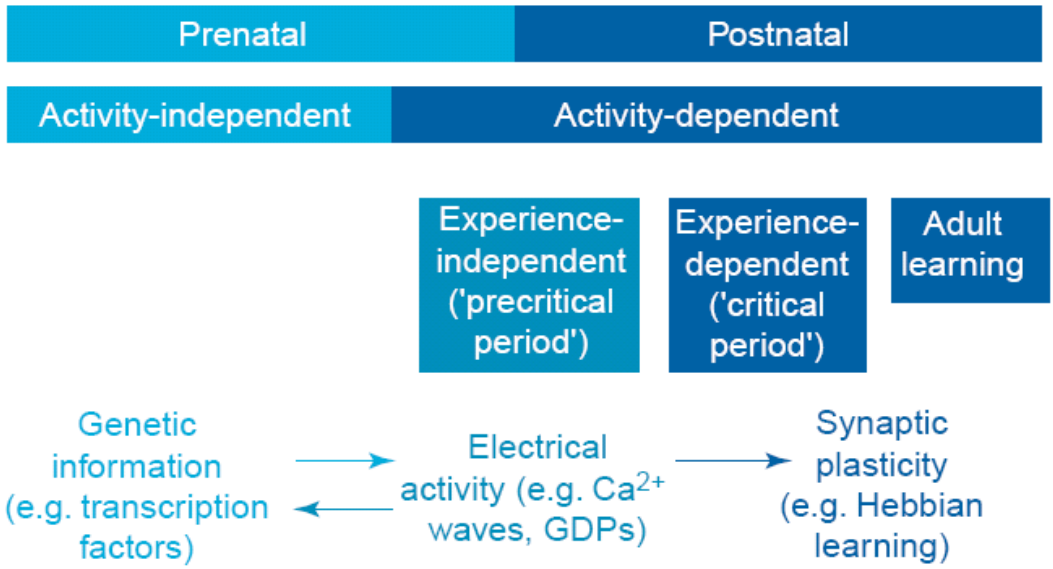

Figure 1. Formation of early neuronal networks relies on genetic information and on electrical activity. During embryonic development, immature neuronal circuits are established on the basis of genetic information. Afterwards, different types of perinatal neuronal activity play the determining role for tuning the development of neuronal networks. During further postnatal development (e.g. during "critical periods"), the network is modulated in an experience-dependent manner based on Hebbian learning rules (Hebb, 1949). Picture adapted from Khazipov and Luhmann (2006).

The events of early neuronal networks include the establishment of the primordial nervous system in the embryo, the initial generation of neurons from precursor cells, the formation of the major brain regions, and the migration of neurons

from the sites of generation to their final positions (Figure 2, Bloom et al., 2002) (for review, see Kriegstein and Noctor, 2004). The stem cells of the ventricular zone (VZ) produce both neurons and glial cells. Some early born neurons built the preplate (PP) which will be split into marginal zone (MZ) and subplate (SP) in an inside-out order (Kriegstein and Noctor, 2004). Neurons migrate to invade the cortical plate (CP) along radial glia using gap junction adhesion (Elias et al., 2007). The radial glial cells, like the neuronal stem cells, can generate daughter neurons (Noctor et al., 2001) and become subsequently matured glial cells (Marshall et al., 2003a). In the neonate, the CP develops the layers II to VI. The transient SP in P0 mice develops to be deeper part of layer VI (Bloom et al., 2002;Allendoerfer and Shatz, 1994).

In the cortex one can find two different neurons: the interneurons and the pyramidal neurons. The interneurons migrate from the ventral telencephalon to the cortex (for review, see Kriegstein and Noctor, 2004;Wonders and Anderson, 2006). The pyramidal neurons migrate to the cortex via radial glial cells (Rakic, 1972) (for review, see Kriegstein and Noctor, 2004). Subventricular zone (SVZ) progenitors generate clones containing both astrocyte and oligodendrocyte precursors (Marshall et al., 2003a). Microglial cells are the third kind of glial cells, which are considered to derive from cells of the monocytic lineage and invade the brain early in development (for review, see Farber and Kettenmann, 2005).

The formation of oscillations

Richard Caton (1842-1926) of Liverpool, England was the first scientist who discovered the electrical nature of the brain in animal subjects (Caton, 1875) and laid the groundwork for Hans Berger to discover Alpha wave activity in the human brain (Berger, 1929). These early works have inspired the classification of brain oscillations into a family of frequency bands, with correlated with mental and/or behavioral activity.

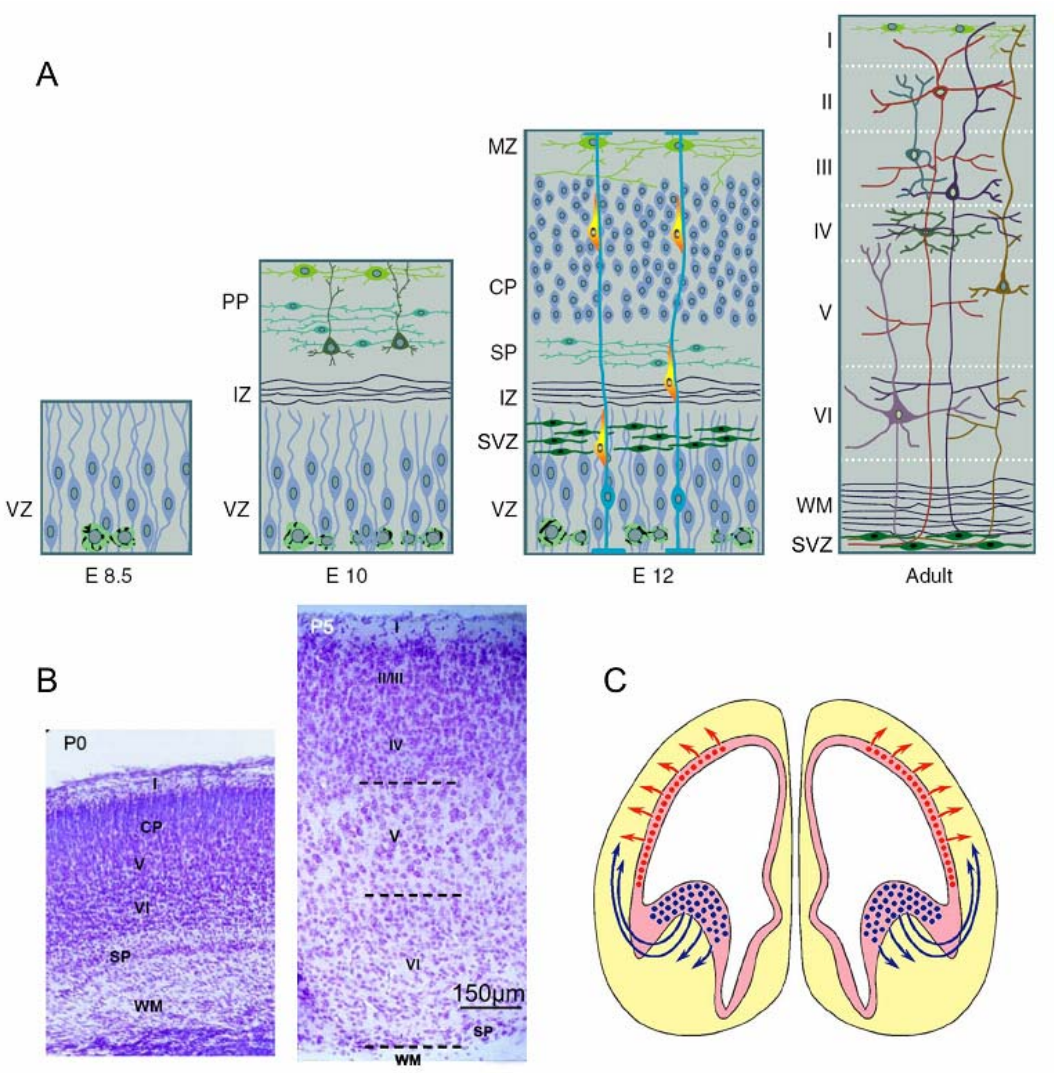

Figure 2. The formation of the cerebellar neocortex. (A) Neurons proliferate in the ventricular zone (VZ). Some early born neurons built the preplate (PP) which will be split into marginal zone (MZ) and subplate (SP). Neurons born in the VZ migrate vertically to invade the cortical plate (CP) along radial glia. In the neonate, CP develops the layers II - part of IV. (B) Nissel staining of neocortex of mouse in P0 and P5. The SP in P0 develops to be the deeper part of layer VI. (C) The pyramidal neurons (red) migrate to the cortex along radial glial cells (radial migration), while the interneurons (blue) migrate from the medial ganglionic eminence in a horizontal manner to the cortex (tangential migration). Picture adapted from Bloom et al., (2002).

Recordings of the electrical activity of the cerebral cortex through electrodes placed on the scalp are called electroencephalogram (EEG) (Purves et al., 2001). In contrast, recordings of neuronal activity with electrodes close to specific layers of cortex or nucleus, are called local field potential (LFP) (Windhorst and Johansson, 1999). The field potential is based on the integration of excitatory postsynaptic potential (EPSP) of neurons. In order to obtain a LFP neurons have to be arranged in a parallel orientation, such as in the cortex or hippocampus. When all these orientated neurons receive synaptic inputs, the extra-cellular signals do not average out, but rather add up to give a signal that can easily be recorded as a LFP. (http://en.wikipedia.org/wiki/ Excitatory_postsynaptic_potential).

While neurons synchronize and resonate with precision in the millisecond range, the field potentials show certain frequency bands of oscillations (Buzsaki and Draguhn, 2004), which are divided into five major frequency bands: delta (δ, 0.5–4 Hz), theta (θ, 4–8 Hz), alpha (α, 8–13 Hz), beta (β, 13–30 Hz) and gamma (γ, 30–80 Hz). Neighboring frequency bands, obtained from the same neuronal network, are associated with different brain states and compete with each other (Engel et al., 2001). These different rhythms are shaped by inhibitory GABAergic interneurons (for review, see Buzsáki and Chrobak, 1995), which constitute 15%–20% of the population of all cortical neurons (for review, see Markram et al., 2004). The inhibitory GABAergic interneurons are partially coupled via gap junction (for review, see Ascoli et al., 2008;Elias and Kriegstein, 2008), which contributes to the synchronization between coupled interneurons and further coordinates the firing of pyramidal cells (for review, see Fukuda, 2007). In contrast, pyramidal neurons do not use gap junctions for directly communication except during the early postnatal period (Schmitz et al., 2001;Fukuda, 2007).

Depending on the brain's state the EEG differs in amplitude and frequency (Figure 3). The slow oscillations of delta (δ, 0.5–4 Hz) rhythm are associated with a slow-wave sleep, sleep spindles or non-REM (rapid eye movement) sleep (for review, see Sejnowski and Destexhe, 2000). The non-REM sleep is characterized by high amplitude and low frequency. Episodes of REM sleep has a main frequency in the theta band (θ, 4–8 Hz), in this period the motor output is markedly inhibited (Sejnowski and Destexhe, 2000). During sleep, the cortex alternates between periods

of slow-wave sleep of delta (δ, 0.5–4 Hz) rhythm and episodes of REM sleep of theta (θ, 4–8 Hz) rhythm.

Alpha (α, 8–13 Hz) rhythm, which was first recorded by Berger (1929), is associated with relaxed wakefulness and is enhanced in the visual cortex when the eyes are closed (Buzsáki, 2006). Similarly, in somatosensory cortex, mu rhythm, which is in Alpha range, is referred to as a motor-relaxation-associated rhythm (Buzsáki, 2006).

Upon arousal the low-frequency oscillations disappear and are replaced by higher frequency rhythms including beta (β, 13–30 Hz) and gamma (γ, 30–80 Hz) rhythm, which are typical of active and awake states (Sejnowski and Destexhe, 2000). Gamma (γ, 30–80 Hz) rhythm has been observed during attention, learning, and perception (Engel et al., 2001;Buzsáki, 2006).

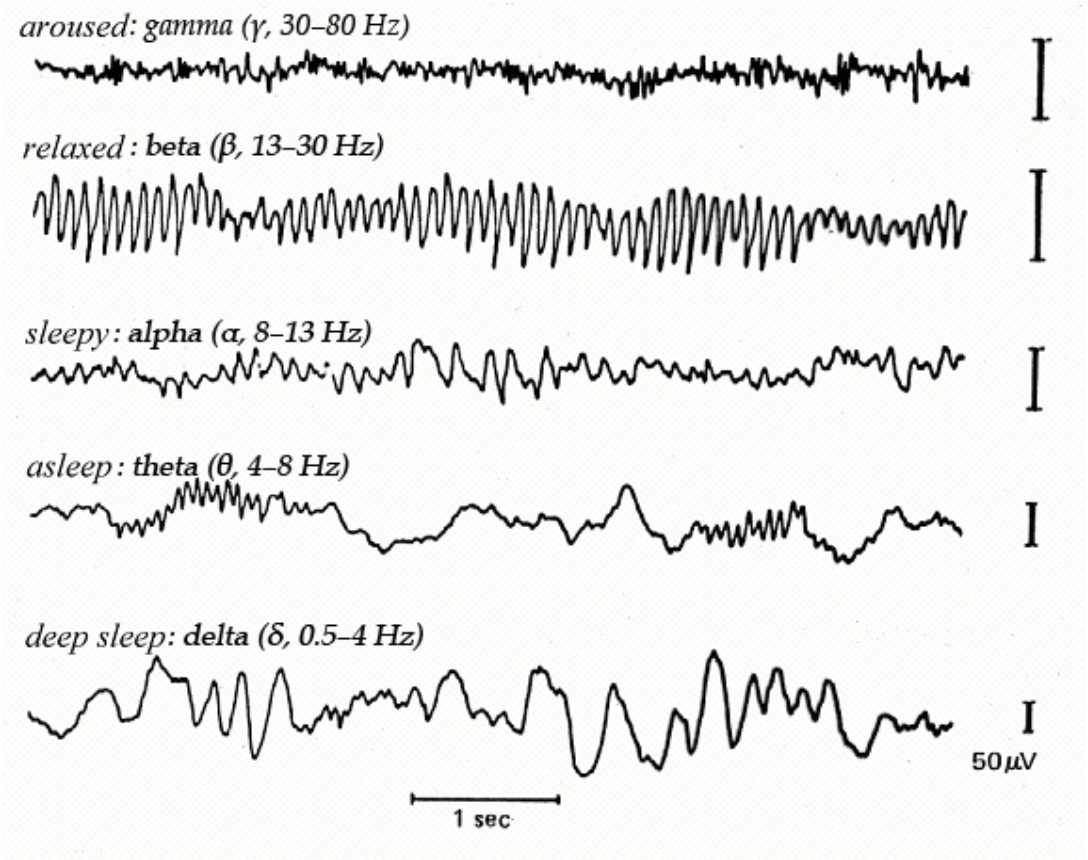

Figure 3. EEG rhythms in humans. Depending on the brain's state the EEG differs in amplitude and frequency. Picture modified from http://neurocog.psy.tufts.edu/.

Spontaneous oscillations in the early stages of development

Synchronized network oscillations have been observed during early stages of development in a variety of neuronal structures, such as the spinal cord (for review, see Spitzer, 2002), retina (for review, see Huberman et al., 2008), hippocampus (for review, see Le Van et al., 2006) and cerebral cortex (for review, see Khazipov and Luhmann, 2006); (for a comprehensive review Moody and Bosma, 2005). These transient oscillations cause a prominent increase in the intracellular calcium concentration, which subsequently regulates gene expression (for review, see Fields et al., 2005). Specific activity patterns, which play essential roles in many aspects during embryonic and perinatal development (for review, see Spitzer, 2006), regulate specific genes. These genes control neuronal differentiation and neurotransmitter specification (for review, see Spitzer et al., 2004), modulate proliferation (Weissman et al., 2004;Liu et al., 2005), growth and remodeling of dendrites (for review, see Lohmann and Wong, 2005;Redmond and Ghosh, 2005), neuronal migration (for review, see Komuro and Kumada, 2005), refinement of axonal projections (for review, see Firth et al., 2005) and apoptosis (for review, see Hara and Snyder, 2007).

Spontaneous oscillations and the formation of early neuronal networks

A number of *in vitro* and recent *in vivo* studies have described the patterns of synchronized network oscillations in the cerebral cortex of newborn rodents. Spontaneous (Garaschuk et al., 2000;Corlew et al., 2004a) as well as neurotransmitter-evoked (Flint et al., 1999;Peinado, 2000;Calderon et al., 2005) calcium waves propagate over large areas across the immature cerebral cortex. Calcium imaging studies also revealed the columnar arrangement of co-active, gap junction-coupled neurons in so-called neuronal domains of 100–200 µm in diameter (Yuste et al., 1995;Kandler and Katz, 1998). This columnar arrangement could be recently confirmed with multiple extra-cellullar recordings in the intact cerebral cortex of the newborn rat (Kilb and Luhmann, 2003) and mouse (Dupont et al., 2006). In this intact *in vitro* preparation activation of muscarinic acetylcholine or metabotropic glutamate receptors (Wagner and Luhmann, 2006) elicits a transient network oscillation. This reflects the highly synchronized activity of gap junction-

coupled neurons organized in a column of 200 μm in diameter. Recent *in vivo* recordings in the somatosensory cortex (Khazipov et al., 2004;Minlebaev et al., 2007) and visual cortex (Hanganu et al., 2007) of newborn rats have demonstrated spontaneous and periphery-driven, spatially confined spindle burst oscillations.

Spike-dependent neuronal code

Underlying the spontaneous oscillations, spike activity could be obtained using a high-pass filter (Windhorst and Johansson, 1999). Spikes from large numbers of neurons could be recorded via multi-electrode arrays (Blanche et al., 2005). These neurons are situated across large areas and they can become transiently synchronized during oscillations (Ritz and Sejnowski, 1997). Oscillations act as background that brings neurons to the phase of synchronized depolarization (Nadasdy, 2000). During further postnatal development (Figure 1), these synchronized neurons are supposed to carry information according to Hebb's learning rules or cell assemble theory (Hebb, 1949), which suggested that any two cells or systems of cells that are repeatedly active at the same time will tend to become "associated." That means that activity in one cell facilitates activity in the other cell.

Several models of neuronal coding have been imposed (Nadasdy, 2000) (Figure 4 for model 1–4).

(1) In the "rate coding" hypothesis (Rolston et al., 2007) (Figure 4a), which is based on the "integrator" model of neurons, neurons generate different frequency of spikes after stimuli. The firing rates of neurons are related to the stimulus intensity.

(2) In the "temporal coincidence" hypothesis (Gray et al., 1992) (Figure 4b), spikes tend to synchronize at certain frequency range. The information coded in the spike is the temporal coincidence of inputs towards the firing neuron.

(3) According to the "delay coding" hypothesis (Buzsaki and Chrobak, 1995) (Figure 4c), a spectrum of different intensity input signals are converted to different delays of spikes. This model assumes that neurons express synchronous sub-threshold membrane potential oscillation, which allows generating a spike at particular phases of the underlying oscillation. The information is coded in the spike precession within the oscillatory cycle.

(4) According to the "sequence coding" hypothesis (Abeles and Gerstein, 1988) (Figure 4d), neurons generate sequences of spikes with certain delays between the spikes of different neurons. Spikes engaged to a sequence are also expected to coincide with the local field activity. Note that this model integrates both the temporal coincidence and the delay coding.

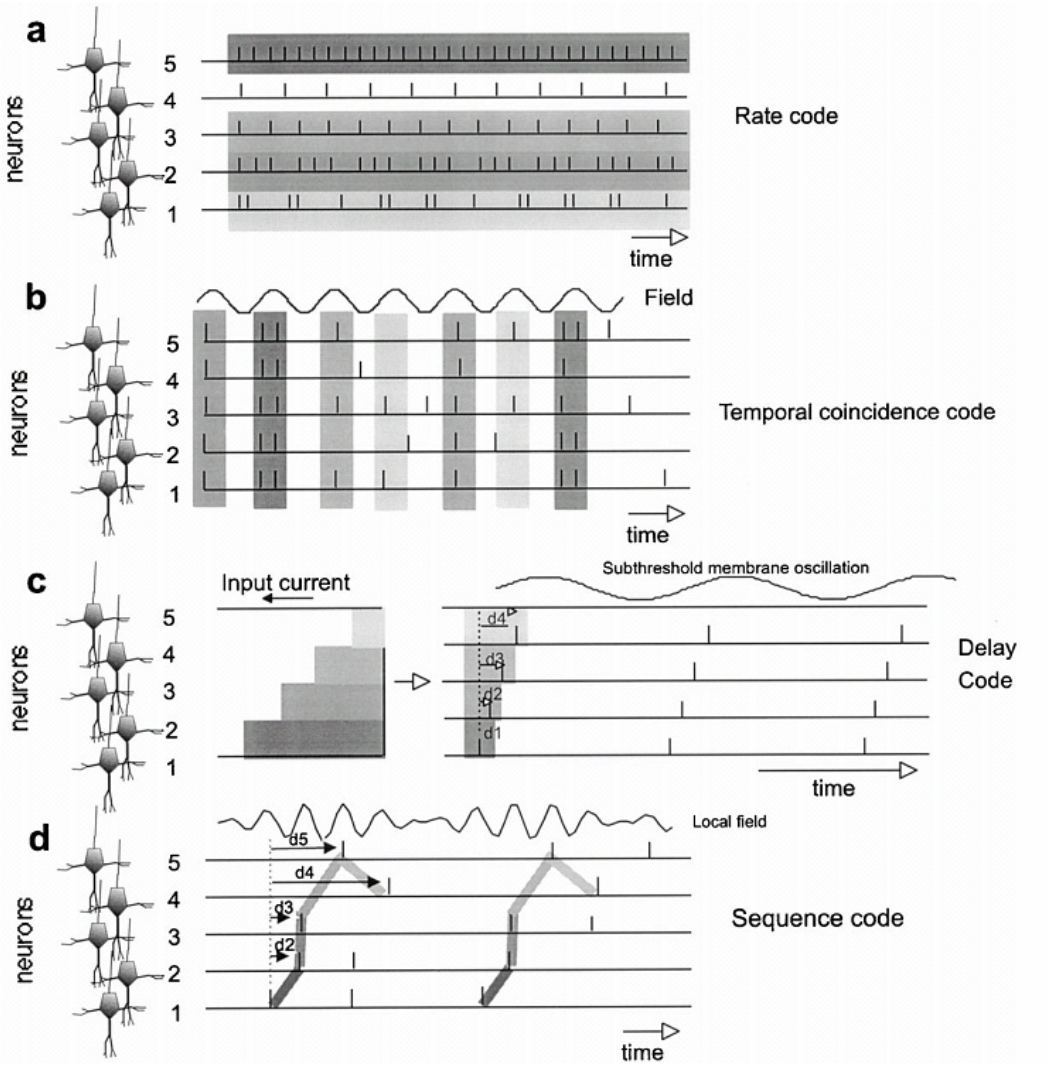

Figure 4. Main models of neuronal coding. (a) In the 'rate coding' hypothesis (Rolston et al., 2007) neurons generate different spiking frequencies. (b) In the 'temporal coincidence' hypothesis (Gray et al., 1992) spikes tend to synchronize at a certain frequency range. (c) According to the 'delay coding' hypothesis (Buzsaki and Chrobak, 1995) a spectrum of different intensity input signals are converted to different delays of spikes within a oscillatory cycle. (d) According to the 'sequence coding' hypothesis (Abeles and Gerstein, 1988) neurons

generate sequences of spikes with certain delays between the spikes of different neurons. Spikes engaged to a sequence are also expected to coincide with the local field activity. Note that this model integrates both the temporal coincidence and the delay coding. Picture adapted from Nadasdy, (2000).

(5) The "phase sequence" hypothesis (Harris, 2005) (Figure 5) is based on the internal cognitive processes (ICPs) of Hebb's theory (Hebb, 1949). In this hypothesis, the same assembly might be triggered by either sensory inputs or the activity of other assemblies. Sequent assemblies may occur and it is the hypothesized substrate of ICPs.

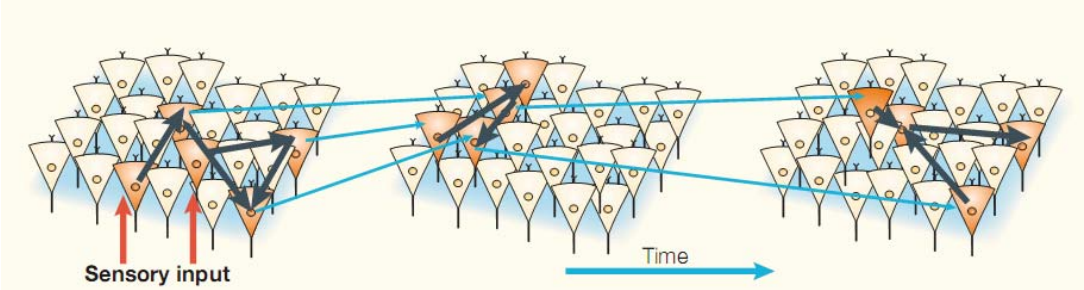

Figure 5. The "phase sequence" hypothesis. Sensory input (red arrows) triggers certain neurons to fire. These neurons transiently drive an assembly of neurons (black arrows), which lead to subsequent activation of a new assembly via inter-assembly connections (blue arrows). The evolution of this phase sequence is the hypothesized substrate of internal cognitive processes. Picture adapted from Harris, (2005).

(6) The "binding theory" hypothesis (for review, see Roskies, 1999) (Figure 6) was summarized by Wolf Singer in the following way: "the representation of the various attributes of the visual world by distributed neuronal assemblies can be bound together harmoniously in the time domain through oscillatory synchrony" (Buzsáki, 2006). As describe in other words: "A simple ball is characterized by a color, a size, a texture, a movement pattern that distinguishes it from other objects. These features are processed in different parts of the cortex and have to be bound together to form an image in the brain to recognize it as a ball even if the perceptual conditions and its characteristics diverge from the model in mind." (Lapray, 2009).

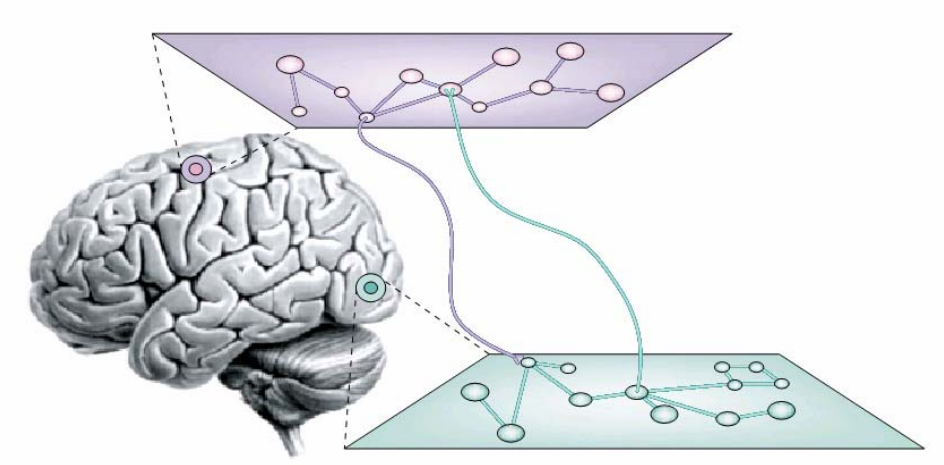

Figure 6. The "binding theory" hypothesis. Features of an objective could be processed transiently in separate neural assemblies with dynamic long-range interactions. Picture adapted from Varela et al., (2001).

Studying the "sequence coding" hypothesis in micro-electrode arrays

Hebb (1949) first proposed activity-dependent learning rules, in which information processing and storage was coded via dynamically linked assemblies of cells. Neuronal assemblies (for review, see Nadasdy, 2000;Plenz and Thiagarajan, 2007), referred in this study to repetitive spike patterns in a population of neurons, similar to "cortical songs", "motifs", or "neuronal avalanches". Repetitive spike patterns have been found in various models and systems, such as *in vivo* (Abeles and Gerstein, 1988;Nadasdy et al., 1999;Fujisawa et al., 2008;Gireesh and Plenz, 2008;Pastalkova et al., 2008) , in brain slice (Ikegaya et al., 2004;MacLean et al., 2005;Gireesh and Plenz, 2008) and in cell culture (Segev et al., 2004;Eytan and Marom, 2006;Madhavan et al., 2007;Rolston et al., 2007;Pastalkova et al., 2008). These works strongly suggest that repetitive spike patterns provide the proof of information storage among neurons.

The *in vitro* model of neuronal culture on micro-electrode arrays (MEA) provides a precise spatio-temporal recording over long periods of time that allows us to study the basic mechanisms of the formation of neural network (Marom and Shahaf, 2002). With the help of this model, a number of studies have shown that growing

dissociated neurons gradually self-organize themselves and assemble to a neural network with complex spiking and recurrent bursts (Droge et al., 1986;Habets et al., 1987;Kamioka et al., 1996;van Pelt et al., 2004;Wagenaar et al., 2006).

Questions

In this thesis, we address the question of how individual neurons associate together to assemble neuronal networks and present spontaneous electrical activity. Therefore, the neonatal brain was dissected and used at three different levels: (1) acute 1-mm thick brain slices, (2) cultured organotypic 350-µm thick brain slices, and (3) dissociated neuronal cultures. The spatio-temporal properties of neural activity were investigated by using a 60-channel MEA with inter-electrode distances of 100 or 200 µm.

(1) **Acute brain slices:** We use a MEA to investigate the spatio-temporal properties of spontaneous, carbachol-induced, and electrical stimulus-induced synchronized network oscillations in somatosensory cortical slices of 1-mm thickness from newborn mice (postnatal day [P] 0–P3).

(2) **Cultured brain slices:** We used cultured organotypic slices, of somatosensory cortex from newborn mice, to study the spatio-temporal properties of spontaneous neuronal activity and their pharmacological mechanisms.

(3) **Dissociated neuronal cultures:** We used the *in vitro* model of cultured cortical neurons on MEA as well as a template-matching algorithm (Abeles and Gerstein, 1988;Schrader et al., 2008) to investigate the neuronal assemblies during 6 to 16 day *in vitro* (div). We were interested in the following questions. (a) Are the appearances of repetitive spike patterns age-dependent during the development? (b) Do neurons play some particular roles in the repetitive spike patterns? (c) Are there any relationships between different repetitive spike patterns?

2. Materials

Chemicals

ACSF for acute slice	$CaCl_2$	1.6 mM
	glucose	10 mM
	KCl	5 mM
	$MgSO_4$	1 mM
	NaCl	124 mM
	$NaHCO_3$	26 mM
	NaH_2PO_4	1.25 mM
	pH 7.4	
ACSF for cultured slice	$CaCl_2$	1.8 mM
	choline chloride	0.028 mM
	D-glucose	25 mM
	glycine	0.4 mM
	KCl	5.36 mM
	L-alanine	0.02 mM
	L-glutamine	0.5 mM
	L-serine	0.4 mM
	(N-[2-hydroxyethyl]-piperazine-N'-[2-ethanesul-fonic acid]) sodium salt	10 mM
	$MgCl_2$ $6H_2O$	0.812 mM
	NaCl	51.3 mM
	$NaHCO_3$	26 mM
	NaH_2PO_4 H_2O	0.9 mM
	sodium pyruvate	0.23 mM
	pH 7.4	
Arabinofuranoside (AraC)	Sigma-Aldrich, Steinheim, Germany	

BME/10%FCS	Basal medium eagle (Gibco) containing 10% fetal calf serum	
Minimal Essential Medium (MEM)	Gibco, Invitrogen, Carlsbad, CA	
NB/N27	Neurobasal medium	
	B27	2% (Gibco)
	glutamax	2 mM (Gibco)
	penicilline/streptomycine	10 µg/ml
Modified phosphate buffered saline without Ca^{2+} and Mg^{2+} ($MPBS^{-/-}$)	BSA	1 mg/ml
	DNAse I	6 µg/ml
	glucose	10 mM
	glutmax	1 mM
	Hepes	10 mM
	NaOH	4 mM
	penicillin/streptomycin	10 µg/ml
	phenol red (sodium salt)	5 mg/l
	Pyruvate	1 mM
Poly-ornithin	Sigma, Steinheim, Germany	
Trypsin	Sigma–Aldrich, Steinheim, Germany	

Equipment

ALA MEA-SHEET	ALA scientific Instruments, NY, USA
Anti-vibration table	Institute of Physiology, Mainz, Germany
Inverted microscope	Optika microscopes, Bergamo, Italy
MEA 1060-INV-BC interface	Multi Channel Systems (MCS), Reutlingen, Germany
MEA chips	Ayanda Biosystems, Lausanne, Switzerland
Millicell-CM membranes	Millipore, Bedford, MA
Nikon Coolpix 4500	Nikon , Tokyo, Japan
Temperature control unit (TCO2 and TH01)	Multi Channel Systems (MCS), Reutlingen, Germany
Tissue chopper	McIlwain, Mickle Laboratory Engineering, Surrey, UK
Vibroslicer	TPI, St Louis, MO, USA

Software

Corel Draw 12	Corel GmbH, Unterschleiβheim, Germany
Excel MS Office 2000	Microsoft, Redmond, USA
Matlab 7.2	The MathWorks Inc., Natick, USA
MC_SELECT	Multi Channel Systems (MCS), Reutlingen, Germany
MC_STIMULUS	Multi Channel Systems (MCS), Reutlingen, Germany
MC_RACK	Multi Channel Systems (MCS), Reutlingen, Germany
Photoshop CS	Adobe Systems Inc., CA, USA
Reference Manager Pro 10	Reference Manager, USA
SigmaPlot 2001	SPSS Inc., Chicago, IL
Systat version 10	Systat Software, Erkrath, Germany
Word MS Office 2000	Microsoft, Redmond, USA

3. Methods

Preparation and MEA recording in acute brain slices

All experiments were conducted in accordance with the national and European (86/609/EEC) laws for the use of animals in research, and were approved by the University of Mainz Ethical Committee. Acute 400–1000-µm-thick coronal or sagittal slices including the primary somatosensory cortex were prepared from neonatal C57BL6 mice (P0–P3; day of birth, P0). Newborn mice were anaesthetized by hypothermia and decapitated. The brain was rapidly removed and transferred to oxygenated (95% O_2 and 5% CO_2), ice-cold (2–5 °C) artificial cerebrospinal fluid (ACSF) of the following composition (in mM): NaCl, 124; KCl, 5; $CaCl_2$, 1.6; $MgSO_4$, 1; $NaHCO_3$, 26; NaH_2PO_4, 1.25; glucose, 10 (pH 7.4). Slices were cut in oxygenated, ice-cold ACSF with a vibroslicer (TPI, St Louis, MO, USA) and transferred to an incubation chamber containing ACSF at 32–33 °C. After an incubation period of 1–2 h, slices were transferred to a 3D 60-channel MEA (i.e. Figure 8, inter-electrode spacing 100 or 200 µm, electrode resistance 250–450 kOhm and 600– 900 kOhm, respectively; Ayanda Biosystems, Lausanne, Switzerland) on a MEA 1060-INV-BC interface (i.e. Figure 7, Multi Channel Systems [MCS], Reutlingen, Germany), which was mounted on an inverted microscope (Optika microscopes, Bergamo, Italy) equipped with a digital camera (Nikon Coolpix 4500, Tokyo, Japan). Slices were perfused with ACSF at a rate of 2–3 ml/min held constant at 32 °C by a temperature control unit (TCO2 and TH01, MCS). For a good contact between the slice and the electrodes, a 100 mg anchor, made by stainless steel and nylon lines, was used.

Drugs

The cholinergic agonist carbamylcholine chloride (carbachol, 30–100 µM, Sigma-Aldrich) was prepared in distilled water as stock solution (100 mM), stored at 4 °C and was applied for 30–60 sec via the bathing solution. The gap junction blocker carbenoxolone (100 µM, Sigma-Aldrich) was prepared freshly in ACSF.

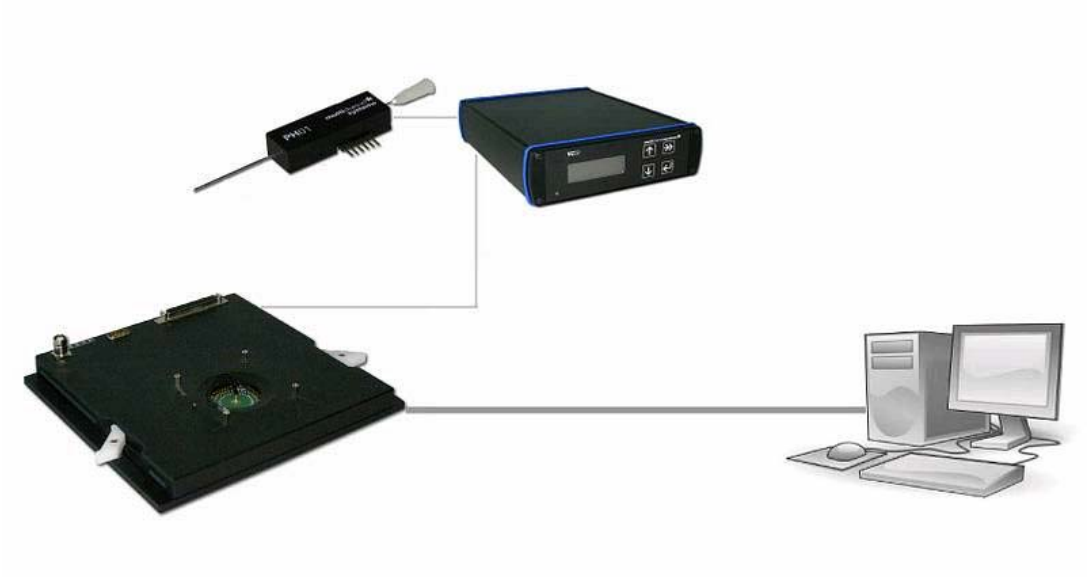

Figure 7. Overview of the MEA setup. The standard MEA setup includes a preamplifier (left-down panel), a perfusion system (upper panel) and an analog-to-digital converter card in a computer (right-down panel). Picture adapted from http://www.multichannelsystems.com/.

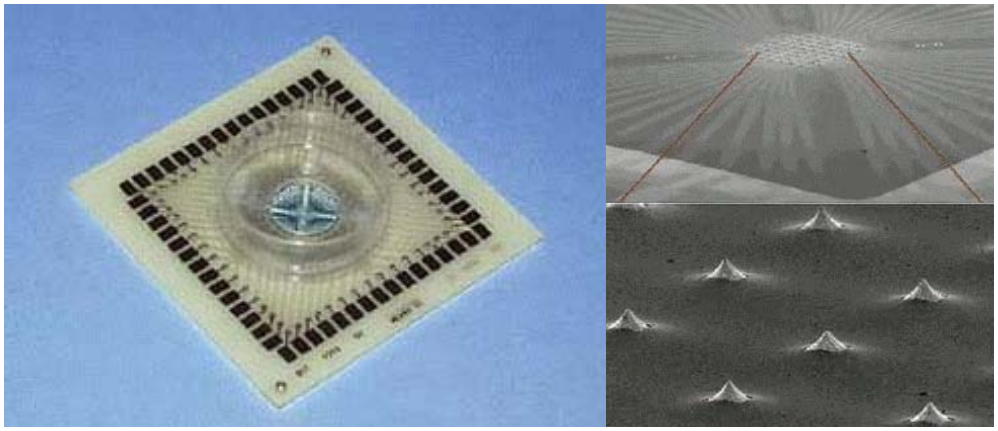

Figure 8. 3-D MEA. Each 3-D MEA has 60 micro-electrodes. The electrode spacing is 100 or 200 µm, electrode height is 25–35 µm or 50–70 µm and electrode dimensions are either 30 µm in diameter or 40 µm x 40 µm. Picture adapted from http://www.ayanda-biosys.com/.

Histology

After the electrophysiological experiments, slices were carefully removed from the MEA and fixed for at least 24 h in 4% paraformaldehyde. Slices were sectioned with a vibratome at 70 µm thickness and Nissl stained. Digital photographs of the cortical slices on the MEA were used to align photographs of the Nissl-stained sections to the 60 recording sites (Figure 15). This procedure allowed the layer-specific identification of each electrode.

Preparation and MEA recordings of organotypic neocortical slice cultures

Organotypic neocortical slices were prepared from newborn (P0) C56 or balbC mice and cultivated according to the Stoppini method (Stoppini et al., 1991). Animals were killed by decapitation and the brain was quickly removed. All subsequent procedures were performed in Minimal Essential Medium (MEM, Gibco, Invitrogen, Carlsbad, CA) supplemented with 2 mM glutamine, pH 7.4 at 4 °C. Neocortical hemispheres were isolated from the hippocampus, thalamus and striatum and 350 µm thick coronal slices containing the somatosensory cortex were cut with a tissue chopper (McIlwain, Mickle Laboratory Engineering, Surrey, United Kingdom). The meninges were carefully removed and the dorsolateral part of the cerebral cortex was dissected with a microscalpel. The isolated somatosensory cortical slices were transferred onto Millicell-CM membranes (Millipore, Bedford, MA) placed in 35 mm petri dishes. Slices were kept at 37 °C at 5% CO_2 in a serum-free medium containing neurobasal medium supplemented with 2% B27 (Gibco), 2 mM glutamax (Gibco) and 10 µg/ml penicilline/streptomycine. After 24 h, 1 µM Arabinofuranoside (AraC, Sigma-Aldrich, Steinheim, Germany) was added to the medium. Culture medium with AraC was renewed every two days, thereafter.

Cultured slices were transferred to 3-D MEA chips (interelectrode distances of 200 µm, electrode diameter of 30 µm; Ayanda Biosystems, Lausanne, Switzerland) on MEA 1060-INV-BC (Multi Channel Systems [MCS], Reutlingen, Germany), which were mounted on an inverted microscope (Optika microscopes, Ponteranica, Italy). Slices were superfused with an ACSF consisting of (in mM) 51.3 NaCl, 26

$NaHCO_3$, 0.9 NaH_2PO_4 x H_2O, 0.812 $MgCl_2$ x $6H_2O$, 1.8 $CaCl_2$, 5.36 KCl, 25 D-glucose, 10 (N-[2-hydroxyethyl]-piperazine-N'-[2-ethanesul-fonic acid]) sodium salt, 0.23 sodium pyruvate, 0.5 L-glutamine, 0.4 glycine, 0.4 L-serine, 0.02 L-alanine, 0.028 choline chloride, and 0.2 µM $Fe(NO_3)_3$ x H_2O equilibrated with 95% O_2 / 5% CO_2 (pH 7.4; osmolarity 205 mOsm). ACSF was continuously perfused at a rate of 2–3 ml/min at a temperature of 28 °C. Field potentials were recorded simultaneously with 60 extracellular electrodes at a sampling rate of 1 kHz using the MEA_RACK software (MCS).

Pharmacology

After 4 to 5 days in culture, the medium was replaced by neurobasal medium without B27 and specific antagonists were added. In controls an equal volume of the antagonist solvent was applied. AraC was omitted during pharmacological treatments of the slices. After incubation periods of 6, 12 or 24 h, slices were fixed for 30 min with 4% PFA.

The following drugs were used: 10 µM 6-cyano-7-nitroquinoxaline-2,3-dione (CNQX, Sigma); 20 µM(±) 3-(2-carboxypiperazin-4-yl)propyl-1-phosphonic acid (CPP, Sigma); 400 nM [(R)-[(S)-1-(4-bromo-phenyl)-ethylamino]-(2,3-dioxo-1,2,3,4-tetrahy- droquinoxalin-5-yl)-methyl]-phosphonic acid (NVP-AMM077, Novartis Pharmaceuticals, Basel, Switzerland); 3 µM ifenprodil (Tocris); 10 µM nifedipine (Sigma); 100 µM gabazine (SR-95531, Sigma); 25 µM Mefloquine (Roche. Drugs were stored at –20 °C and were diluted to the final concentration on the day of experiment.

Preparation and MEA recording of primary cell cultures

Ten cell cultures were established on 60-channel planar MEA (electrode diameter 30 µm, electrode spacing 200 µm; Ayanda Biosystems, Lausanne, Switzerland) from neonatal C57BL6 mice (P0-P1; day of birth = P0) as described previously (Golbs et al., 2007). In brief, the mice were decapitated; the brain was rapidly removed and transferred into glutamine containing Minimal Essential Medium (Gibco, Invitrogen, Carlsbad, CA). After removing the meninges from the hemisphere the cortex was separated from the hippocampus, striatum and thalamic nuclei. Dissociation of the cortex was done by using trypsin followed by titration. Cells were plated at a density of approximately 1000 cells/mm^2 on MEA coated with 1 mg/ml poly-ornithin (Sigma, Steinheim, Germany) at 4 °C for 24 hours. The MEA was sealed with ALA MEA-SHEET (ALA scientific Instruments, NY, USA), a membrane permeable to air, and relatively impermeable to water vapor (Potter and DeMarse, 2001). Cells were cultured in Neurobasal medium (Gibco) supplemented with 2% B27 (Gibco), 1 mM glutamax (Gibco), 25 U/ml penicillin and 25 µg/ml streptomycin (NB/B27) at 37 °C, 5% CO_2. Medium was completely exchanged after 1 day in culture (div) and half of the medium was replaced with fresh medium weekly.

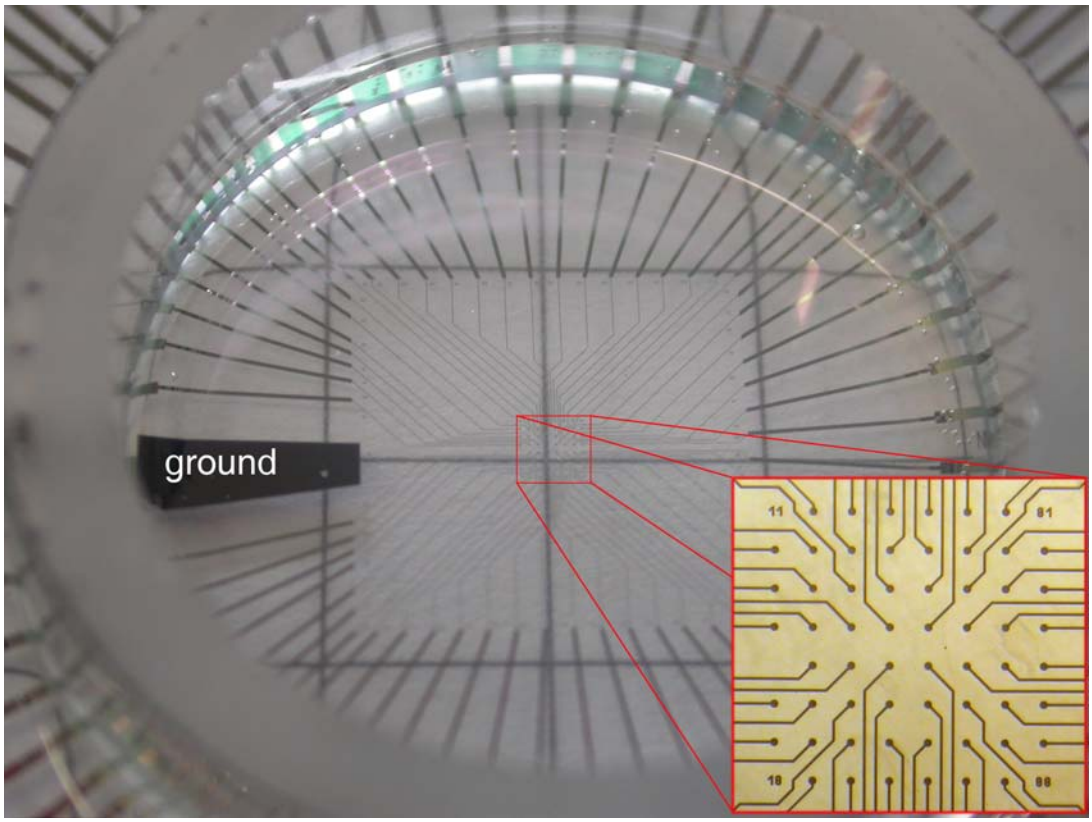

Figure 9. Planar MEA. The planar MEA chip (200/30iR-ITO-gr) has 59 recording micro-electrodes and one internal grounding electrode. The electrode spacing is 200 µm and the electrode diameter is 30 µm. iR: with internal reference electrode; ITO: indium-tin oxide, a transparent conductive metal oxide; gr: glass ring.

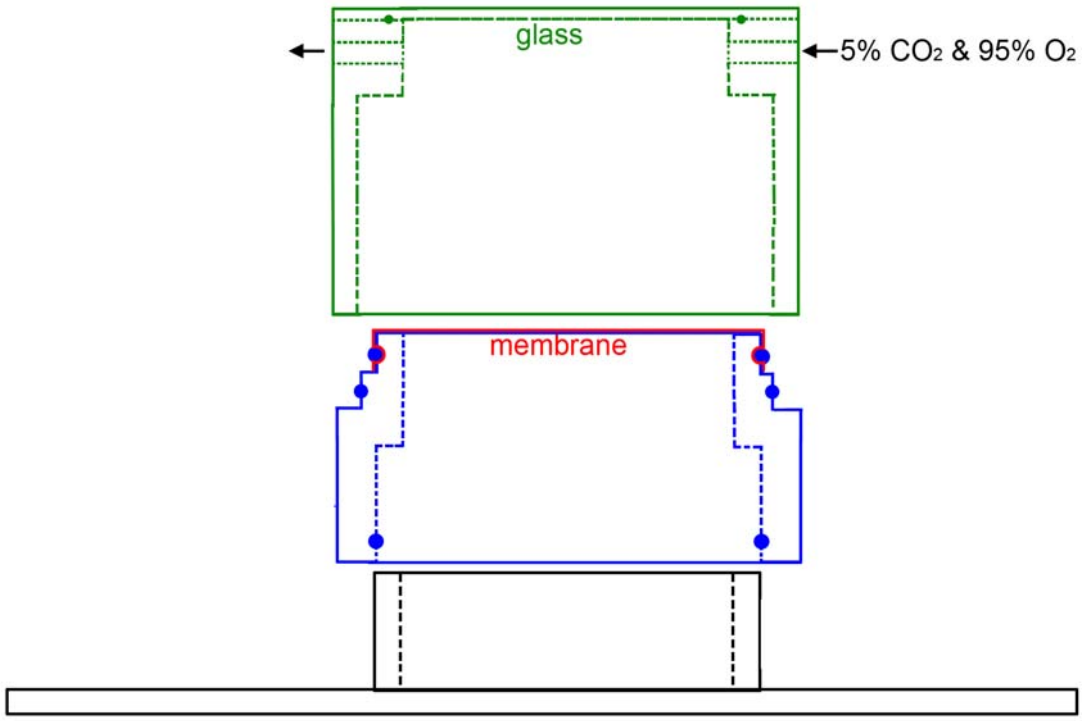

Figure 10. The chamber designed for long-term recording of cell cultures on planar MEA. During the period of cell culture, the MEA chip (black color) is sealed with a lid (blue color), which is sealed with an ALA MEA-SHEET (red color, ALA scientific Instruments, NY, USA), a membrane permeable to oxygen and carbon dioxide, and relatively impermeable to water vapor (Potter and DeMarse, 2001). During the recording, the MEA chip was further sealed with another lid (green color) for maintaining a constant pH value. When the duration of recording exceeded more than half an hour, 5% CO_2 and 95% O_2 was supplied.

Data Analysis

Field potential

Data were imported to a custom-written program in Matlab version 6.5 (Mathworks, Natick, MA, USA), with datastrm.m and nextdata.m (MC_Rack, MCS). Field potentials recorded in all 60 channels were plotted, and oscillatory network activity was analyzed in its duration (interval between onset and end of one complete oscillatory cycle) and amplitude (voltage difference between the maximal positive and negative peak). Time-frequency plots were calculated by transforming field potentials using Morlet continuous wavelet (cwt.m, Matlab), smoothed (smooth.m, Matlab) and normalized to values between 0 and 1 (Torrence and Compo, 1998;Wagner and

Luhmann, 2006); for this Matlab codes see the appendix. Fast Fourier transformation spectra were calculated and oscillations were analyzed in their maximal power. Cross-correlograms and coherence analyses for oscillatory activity between channels were calculated by the use of Matlab, and strengths were quantified by measuring the maximal cross-correlation coefficient and maximal coherence coefficient, respectively.

Spike activity

MEA recording

The extracellular activity of cultured neuronal networks on MEA was recorded by using a MEA 1060-INV-BC interface (Multi Channel Systems [MCS], Reutlingen, Germany). Signals were obtained simultaneously from 59 electrodes with a sampling rate of 25 kHz and a 100-Hz high-pass filter. During the recording, the MEA was sealed with a lid to maintain a constant pH value. The temperature was held constantly at 32 $^{\circ}$C with a temperature control unit (TCO2, MCS). MEA_RACK software (MCS) was used for data acquisition and online spike detection.

Spike detection

Spikes were detected with the MEA_RACK software (MCS) by using a threshold-based detector. Spike waveforms were saved when the potentials exceeded a threshold of 7 times the standard deviation of noise level. Spike dataset, including the spike waveforms as well as the precise time from each spike, was imported into Matlab 7.2 (Mathworks, Natick, MA, USA) for further analyses.

Spike sorting

Spikes were plotted into a 3-dimentional (3-D) figure according to their minimum values, the latencies of the minimum values, and the slopes between maximal and minimal values of waveforms. The spike sorting method is based on an estimated number of clustering by visual inspection of the 3-D distribution followed by a clustering method of k-means algorithm (kmeans.m, Matlab) (Lewicki, 1998) (Figure 11). According to the result of spike sorting, each spike was assigned a neuron number. The new dataset, consisting of the precise time of each spike and its neuron number, was used for the detection of repetitive spike patterns.

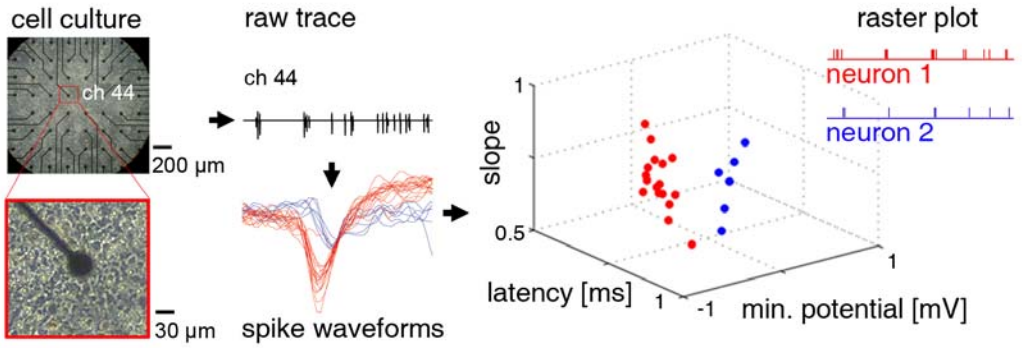

Figure 11. Spike detection and sorting. Recordings were obtained from primary neuronal cultures on planar MEA, which has an electrode spacing of 200 µm. The left-upper panel shows a photograph (x40) of cell culture at 13 div. Data from the channel 44 (enlargement on the left-down panel) are used in the rest of the figure. At each channel a threshold of 7 fold the standard deviation has been used for the spike detection. Three characteristics of spike waveforms were plotted in 3 dimensions, and clustering analysis was done by visual inspection and k-means. Waveforms and raster plots of 2-sorted neurons are displayed in red and blue. Picture from Sun et al., (2009).

Detection of repetitive spike patterns

Repetitive spike patterns were detected by the use of a template-matching algorithm (Abeles and Gerstein, 1988;Nadasdy et al., 1999;Ikegaya et al., 2004;Rolston et al., 2007) (Figure 12A), which is based on the searching of repeating spike sequences between different time windows. These time windows, referred to as template windows, were constructed for each spike with a precision of 2 ms. For the dataset's *i*th spike appearing at time t_i on neuron n_i, a template $temp_i$ was constructed. This vector consists of the latencies and neuron numbers of spikes occurring within 100 ms of t_i. $Temp_i = <t_i\text{-}t_i, t_m\text{-}t_i, t_n\text{-}t_i, \ldots; n_i, n_m, n_n, \ldots>$, in which t_m, t_n,… were between t_i and t_i+100 ms. A match was reported when more than three latency/neuron pairs were identical between different templates. However, the matches from the same neuron were excluded (for the Matlab code, see the appendix). The statistical significance of observed repetitive spike patterns was evaluated by comparing the repetition of the original patterns with the repetition of the surrogates generated by spike shuffling

(Figure 12C and D). Two procedures of spike shuffling, time jittering and neuron jittering (Figure 12B), were used.

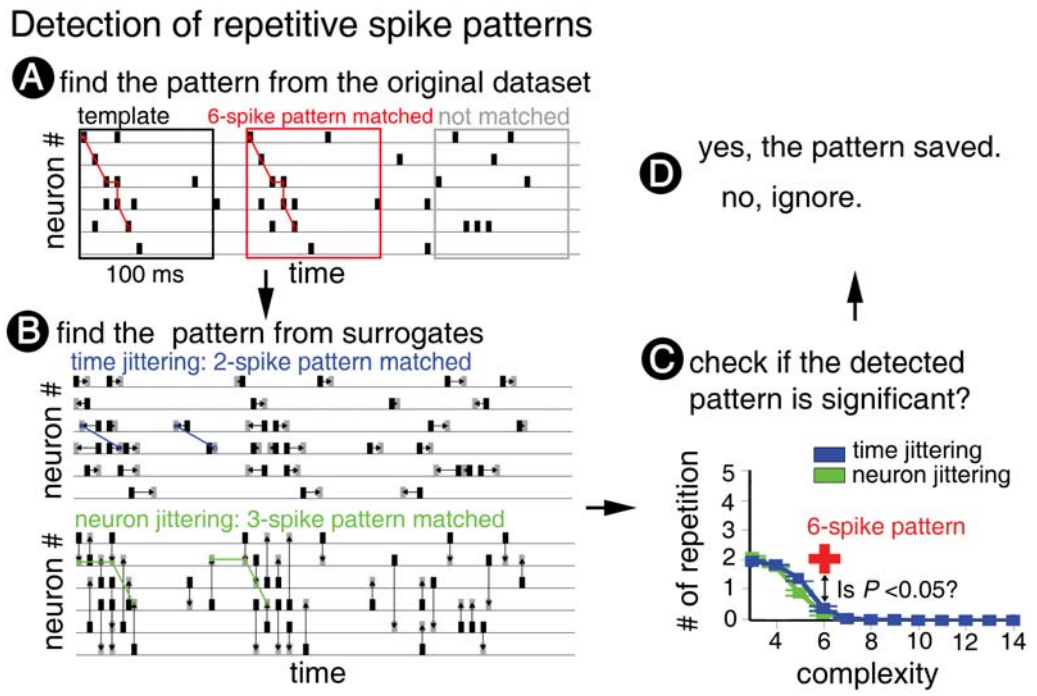

Figure 12. Detection of repetitive spike patterns. (A) Schematic drawing of the basic principle of template-matching algorithm. The black frame shows a time window of 100 ms aligned to the first spike. This window was shifted from spike to spike along the dataset with a precision of 2 ms. The red frame illustrates a matched spike pattern of 6 spikes, while the gray rectangle shows a timeframe without matched pattern. (B) The statistical significance of observed repetitive spike patterns was evaluated by comparing the repetition of the original patterns with the repetition of the surrogates generated by spike shuffling. Surrogate data sets were generated by jittering the time (gray tics) or by changing the neuron numbers (gray tics) of each spike (see Material and Methods). Examples of 2-spike pattern (in blue line) in time-jittered surrogate and 3-spike pattern (in green lines) in neuron-jittered surrogate are illustrated. (C) Only repetitive spike patterns with complexity and repetition (in red +) significantly (z-test, $p < 0.05$) higher than surrogates (time jittering in blue and neuron jittering in green) were saved for further analysis (D). Picture from Sun et al., (2009).

The time jittering method described by Roston and colleagues (2007) was used, wherein each spike's time was disturbed by a random number from a Gaussian distribution with mean zero and 5 ms of standard deviation (SD). Although higher values of SD caused much more reduction in the number of repetitive spike patterns (Figure 13A), the 5 ms of standard deviation was determined by cross-correlation analyses, where the correlation coefficient of the original spike trains did not differ from that by 5 ms of time jittering (t-test, n=100 trials, Figure 13B). The 100 trials for surrogates were chosen regarding to their relative lower standard error (Figure 13A). As the disturbing Gaussian distribution has a mean of zero, the modulations in firing rate are on average unaltered (Figure 13C left panel). Similarly, the inter-spike interval (ISI) distributions for each cell and for the average remain closely preserved (Figure 13C middle and right panel respectively).

The second shuffling method, neuron jittering, changed the neuron number of each spike to a random number, which had the form of a Gaussian distribution with a mean of zero and a standard deviation of one. The principle of this method is identical with the time jittering method. The minimal value, one for standard deviation, was used, since the correlation coefficients between the original spike trains did not differ from that of any neuron jittering (t-test, n = 100 trials, Figure 13B). The dataset retains an identical spike firing rate (Figure 13D left panel) after shuffling, but the cumulative plot of ISI revealed the significant differences (t-test; *, $p < 0.05$) on average (Figure 13D middle panel) and individual traces of ISI (Figure 13D right panel).

Regarding the limited calculation capabilities from the computer, we scanned the repetitive spike patterns from datasets including 3000 spikes. In the subsequent data we only investigated whether identified repetitive spike patterns reappeared. Due to this limitation the total number of repetitive spike patterns is most likely underestimated.

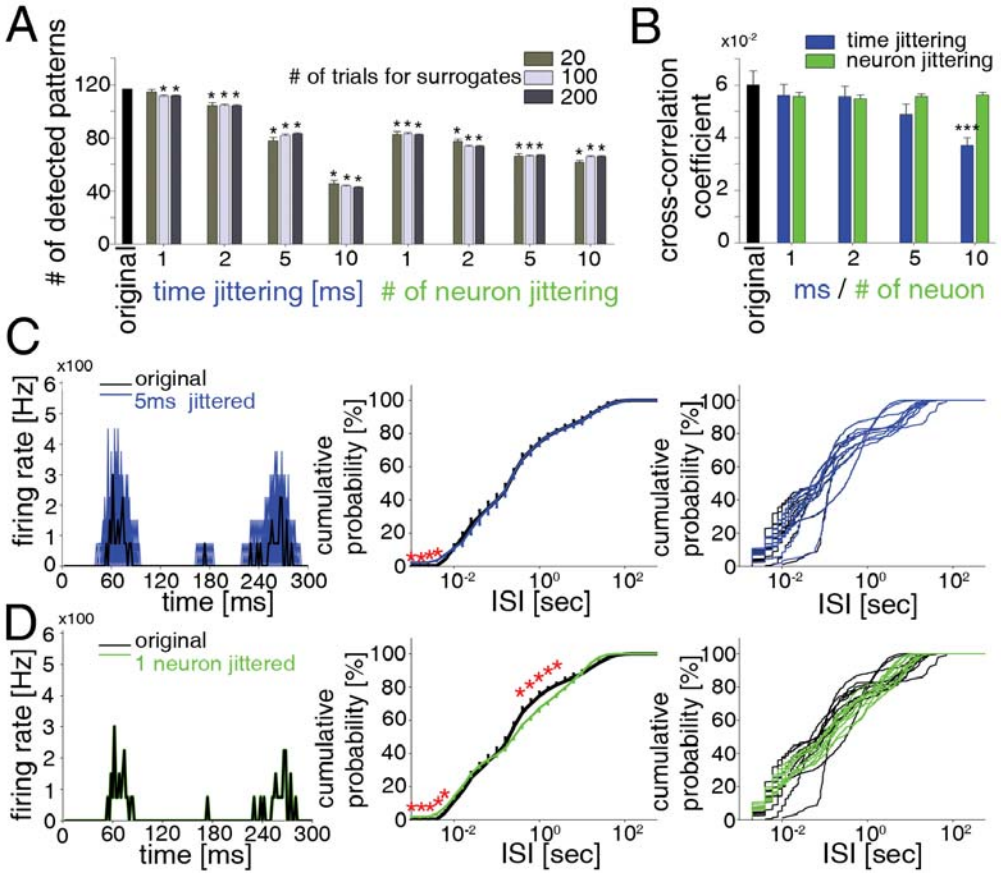

Figure 13. Determination of appropriate surrogate parameters. (A) Black bar represents the number of initially detected patterns from the original data (13 div of figure 25). The bars in the different gray shades represent detected patterns in surrogates created by time jittering of 1, 2, 5 and 10 ms or neuron jittering by 1, 2, 5, and 10 for 20, 100 and 200 trials, respectively (see Material and Methods). A significant (t-test, $p < 0.05$) reduction of pattern numbers is indicated by a *. (B) Cross-correlation analyses between original and surrogates (100 trials). Note that time jittering above 5 ms significantly reduces the cross correlation coefficient, but not in neuron jittering. (C) Effect of 5 ms time jittering on the firing rate and inter-spike intervals (ISI). Because the disturbing Gaussian distribution has a mean of zero, the modulations in firing rate are on average unaltered (left panel). Similarly, the ISI distributions for the average (middle panel) and for each cell (right panel) remain closely preserved. (D) The dataset retains exactly spike firing rate (left panel) after neuron jittering, but the cumulative plot of ISI reveals the significant differences (t-test, *$p < 0.05$) on the average (middle panel) as well as the individual traces of ISI (right panel). Picture from Sun et al., (2009).

Burst detection

Burst detection algorithms described by Raichman and Ben Jacob (2008) were used. A burst is defined as a synchronized event in which several neurons fire in a relatively short time. In our experiments we divided the binary data of each spike train into bins of 200 ms in size and summed up the number of spikes in each bin. As neurons of cultures in immature stage showed only few spikes, bursts including more than 5 spikes were analyzed.

Burst index (BI)

The term "burst index" was used as in the work of Wagenaar (2005), which quantifies the level of burst of spike trains. We divided the binary data of the spike trains into bins of 1 sec in size and summed up the number of spikes in each bin. The bins were sorted by their values. Then the fraction, f_{15}, was derived from the total number of spikes by the number of spikes in the first 15% of sorted bins. If most spikes occurred in bursts, this fraction, f_{15}, was close to one. Conversely, if spikes were sparsely distributed in time, f_{15} was close to 0.15. The burst index (BI) was defined as $BI = (f_{15}–0.15)/0.85$, which was normalized between 0 (no bursts) and 1 (all spikes in bursts).

Hub neurons, lead neurons and stop neurons

In order to investigate the existence of neurons having the same functions within different repetitive spike patterns, we analyzed the spike sequences of all patterns in one recording. Three particular neurons were examined: hub neurons, lead neurons and stop neurons.

Hub neurons were defined as highly connected neurons (Morgan and Soltesz, 2008), which participate in more connections than the average neuron. The connection of each neuron was summed up from the spike sequences of all repetitive spike patterns, where the first and the last neuron of the spike sequences were assigned one connection and the other neurons between were assigned two connections. Neurons which have a significantly higher connectivity ($p < 0.05$, z-test) were defined as hub neurons.

Lead neurons and stop neurons were defined as neurons which generate the first and the last spikes in more repetitive spike patterns, respectively, as the average

neuron. Therefore, the numbers of neurons participating in the first and the last spikes in all repetitive spike patterns were summed up separately. Neurons which have significant higher counts (which mean that they were more often generating the first and last spike than the average neurons) were identified as lead neurons and stop neurons, respectively. The statistic significance was examined by z-test ($p < 0.05$) shown in Figure 14.

Functional connectivity

Functional connectivity (Segev et al., 2004;Baruchi et al., 2008) was defined as the correlations between the activity of individual neurons. In our study it was derived from all identified repetitive spike patterns in one recording. The neuronal correlation matrix NC (m, n) indicated the summation of correlations between $neuron_n$ and $neuron_m$ from all repetitive spike patterns. For example, for the *i*th spike of $neuron_m$ and the *(i+1)*th spike of $neuron_n$ in the spike sequence from *k*th repetitive spike pattern, a value of one was given to NC (m, n). The map of functional connectivity (i.e. Figure 27) was constructed according to the neuronal correlation matrix. The weight of lines indicated the values of neuronal correlations derived from the repetitive spike patterns in one recording.

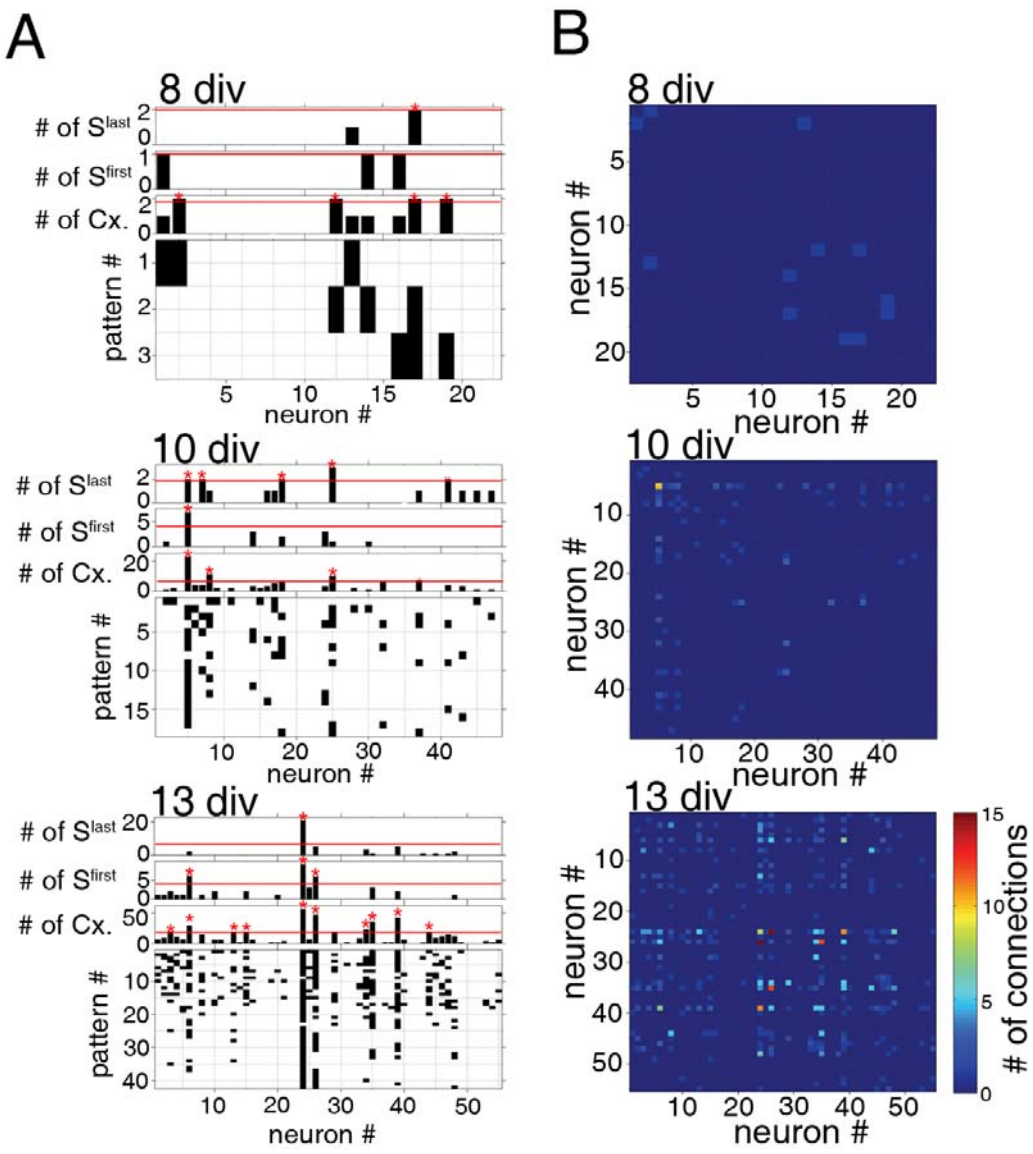

Figure 14. Detections of hub, lead and stop neurons and neuronal connections. (A) The detections of hub, lead and stop neurons, which were defined in the section of Material and Methods, were performed at 8, 10 and 13 div respectively. The numbers of connections (Cx.) of individual neurons and the numbers of neurons participating in the first (S^{first}) and the last spikes (S^{last}) in all patterns are summed up distinctively. The neurons having significantly higher numbers (marked in red *, $p < 0.05$, z-test, red lines mean the 99.5% confidence interval) of connections and generating the first and the last spike of repetitive spike patterns are identified as hub, lead and stop neurons, respectively. (B) The numbers of neuronal connections, which are based on the sequences of repetitive spiking patterns (see Material and Methods), were coded in color. The color maps at 8, 10 and 13 div are illustrated. Note that at 13 div apparent higher values of neuronal connections are observed. Based on the numbers of

neuronal connections, the corresponding maps of functional connectivity are illustrated in Figure 27. Picture from Sun et al., (2009).

Detection of primary and merged patterns

A primary pattern was defined as a repetitive spike pattern which participated in much more different patterns than the average in one recording. The number of each pattern which participated in different patterns was computed by comparing its spatio-temporal spike sequences with that of other patterns. The patterns which have significant higher numbers ($p < 0.05$, z-test) were identified as primary patterns.

In addition, we defined a merged pattern as a repetitive spike pattern which had much more different patterns involved than the other patterns in one recording. The number of each pattern which had different patterns involved was computed by comparing its spatio-temporal spike sequences with that of others. The patterns which have significant higher numbers ($p < 0.05$, z-test) were identified as convergent patterns.

Statistics

For statistical analyses, we use one-way analysis of variance (ANOVA) followed by a Dunnett post hoc test. Values throughout this report are given as mean ± SEM. Significant differences were determined by t-test or z-test. Z-test depends on z-test values, conducted from mean+nSTDs*STD/$n^{1/2}$, where nSTDs = 1.96, 2.58 and 3.3 is correlated to p values of 0.05, 0.01 and 0.001 respectively.

4. Results

Spatio-temporal dynamics of oscillatory network activity in the acute neonatal mouse cerebral cortex

Spatio-temporal properties of spontaneous oscillatory network activity

The spatio-temporal properties of spontaneous network oscillations in newborn (P0–P3) mouse somatosensory cortex were studied with 60-channel MEA chips in acutely prepared slices. We never observed large-scale network oscillations in slice preparations of conventional thickness (400 µm, n=13 slices). Synchronized oscillatory network activity could be only observed in slice preparations of at least 600 µm thickness or in intact cortices (Dupont et al., 2006). In 28 out of 123 somatosensory cortical slices (22.8%) with a thickness between 600 and 1000 µm we could record in 5 mM extracellular potassium prominent spontaneous field potential oscillations (Figure 15). The incidence of network oscillations correlated with the thickness of the slices. Whereas only 11 out of 71 slices (15.5%) with a thickness of 600–800 µm revealed spontaneous network oscillations, 16 out of 51 slices (31.4%) with a thickness of 1000 µm showed prominent synchronized activity. These data indicate that a neuronal network of sufficient 3D size is required to generate this type of early neocortical activity. The incidence of large-scale network activity also depended on the extracellular potassium concentration. Whereas only one out of 17 (5.9%) 1000-µm-thick slices studied in 3 mM KCl revealed robust synchronized network oscillations, six out of 13 slices (46%) with the same thickness but recorded in 8 mM KCl showed network oscillations. All subsequent data were obtained from somatosensory cortical slices of 1000 µm thickness and were recorded in 5 mM extracellular potassium. Under these experimental conditions, spontaneous network oscillations could be recorded at an average interval of 15.4 ± 3.2 min (n=31 oscillations in 11 slices) during observation periods of 2–3 h. Two different patterns of spontaneous activity, local non-propagating (Figure 15) and propagating ones (Figure 16), could be observed. Local non-propagating spontaneous oscillations could be observed in nine out of 16 slices (56%).

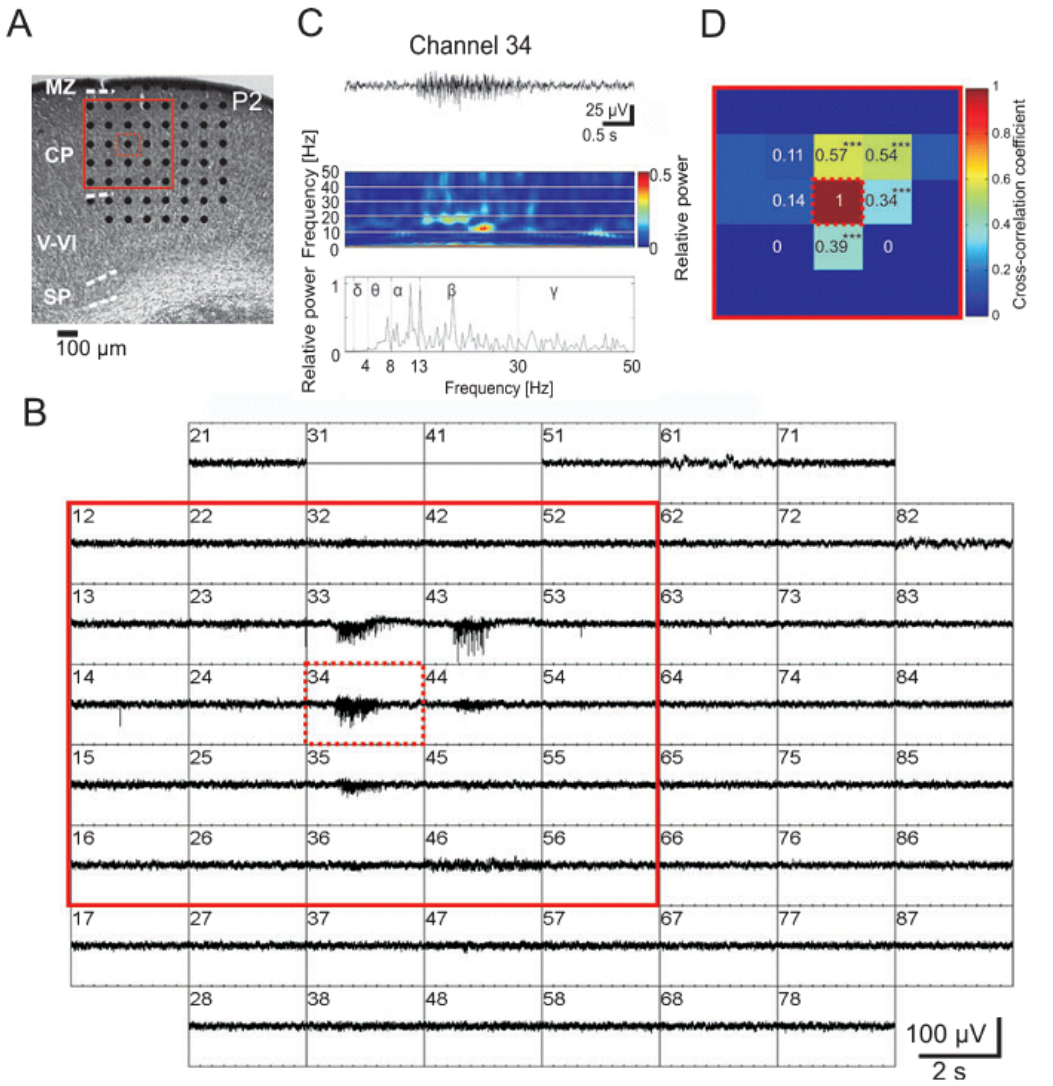

Figure 15. Local, non-propagating spontaneous network oscillations in the newborn mouse somatosensory cortex. (A) Photograph of Nissl-stained coronal slice of the somatosensory cortex from a P2 mouse. Marginal zone (MZ), cortical plate (CP), layers V–VI, subplate (SP) and position of the 60-channel MEA are illustrated. (B) MEA recordings from the 1000-µm-thick slice shown in (A). Spontaneous oscillatory activity can be observed at five recording positions in the CP. Channel numbers 31 and 41 did not function properly, and were turned off. The spacing between electrodes is 100 µm (see scale bar in A). (C) Extracellular recording at electrode number 34 (dotted red square in A and B) shown at higher resolution. The panels below show corresponding wavelet analysis and Fourier spectrum. (D) Cross-correlation analysis of the 25 channels marked in (A) and (B) by a red square. Color code and numbers give the cross-correlation coefficient of each channel in comparison to channel number 34 in the middle position. Asterisks in (D) indicate significantly higher cross-

correlation values (***$p < 0.001$) in comparison to channel 34 (z-test). Note the high cross-correlation between recordings separated from central channel 34 by maximal 100 µm. Picture from Sun and Luhmann, (2007).

These spontaneous oscillations were spatially restricted to a neuronal network of approximately 200 µm in diameter (Figure 15A and B). Wavelet and Fast Fourier analyses demonstrated a predominance of alpha and beta frequencies in the oscillatory field potential responses (Figure 15C). The local non-propagating network oscillations revealed an average peak frequency of 15.6 ± 2.7 Hz, duration of 1.7 ± 0.3 s and maximal amplitude of 66.8 ± 13.1 µV (n=9). The clusters of synchronized activity with high cross-correlation (> 0.5, Figure 15D) and coherence coefficients (> 0.6) were generally localized in the cortical plate (CP), while oscillatory field potentials recorded in lower cortical layers and in the subplate (SP) were synchronized in a columnar arrangement (Dupont et al., 2006).

The second type of spontaneous network oscillations could be observed in 14 out of 16 slices (87.5%). In these slices the activity propagated over at least 1 mm in the medio-lateral (n=11) or latero-medial (n=3) direction. The propagating speed was significantly ($p < 0.05$) higher in the vertical direction (2.4 ± 1.33 mm/s) than in the horizontal direction (0.11 ± 0.01 mm/s). When compared with the local non-propagating spontaneous activity, the propagating oscillations had a significantly lower peak frequency (10.4 ± 0.8 Hz, $p < 0.05$), longer duration (23.8 ± 4.9 s, $p < 0.01$) and larger amplitude (142.9 ± 18.4 µV, $p < 0.01$; n=14, Figure 16C). Propagating network oscillations were also synchronized in a columnar manner, but as revealed by cross-correlation and coherence analyses these spontaneous oscillations synchronized the activity in a larger neuronal network of 300–400 µm in diameter due to the propagation of the activity in horizontal direction (Figure 16D and F). Seven out of the 16 slices tested in detail (44%) showed local non-propagating as well as propagating spontaneous oscillations.

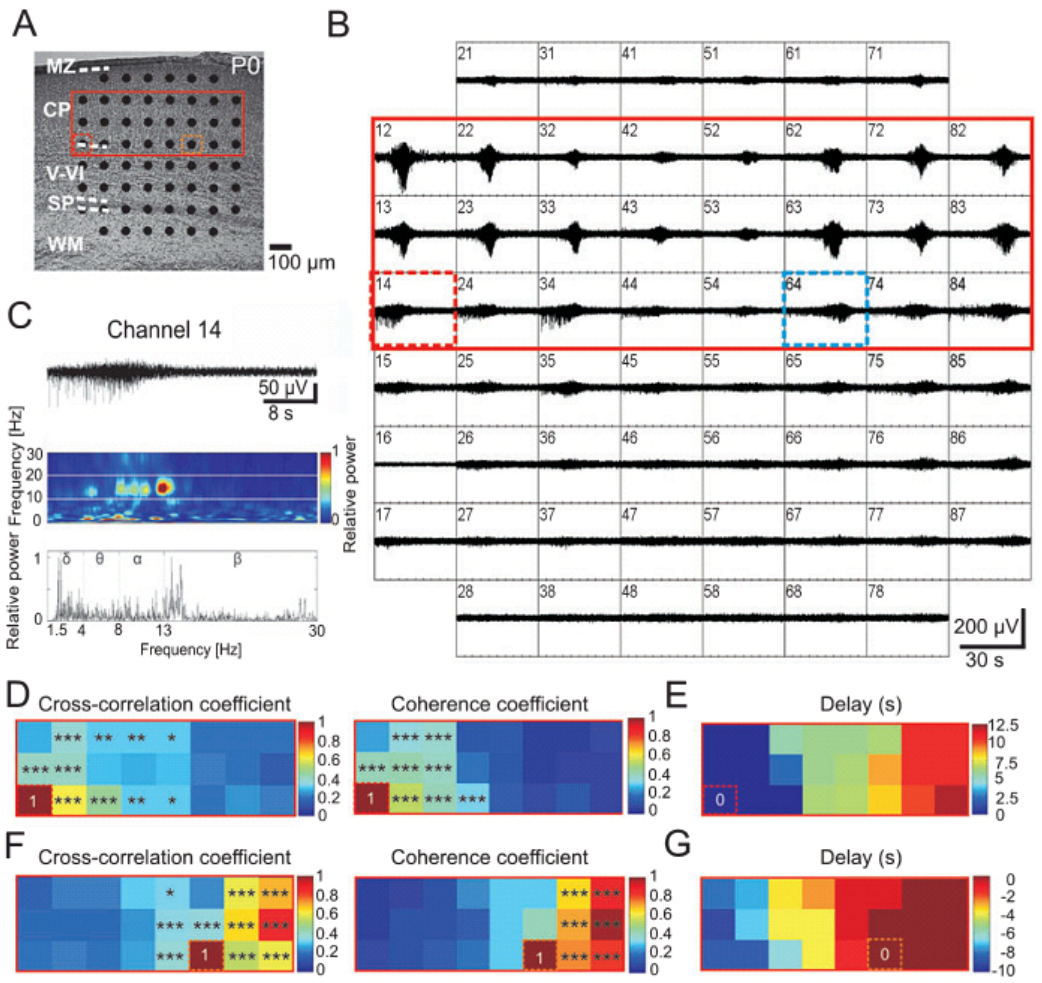

Figure 16. Propagating spontaneous network activity in P0 mouse somatosensory cortex. (A) Photograph of Nissl-stained coronal slice with cortical layers and position of MEA. (B) MEA recordings from the 1000-µm-thick slice shown in (A). Spontaneous oscillatory activity propagated from medial recording sites (channel numbers 12–15) to lateral electrodes (numbers 82–86). The spacing between electrodes is 100 µm (see scale bar in A). (C) Recording at electrode number 14 (dotted red rectangle in A and B) shown at higher resolution with corresponding wavelet analysis and Fourier spectrum. (D) Color-coded plots of the cross-correlation and coherence coefficients for the 24 channels marked in (A) and (B) by a red rectangle. All data were obtained in correlation to channel 14 (lower left corner). (E) Delay of oscillatory activity onset compared with channel 14 in color-coded plot for the same 24 channels as in (D). (F) Color-coded plots of the cross-correlation and coherence coefficients for the same 24 channels as in (D) and (E), but in correlation to channel 64 (dotted blue rectangle in B). (G) Delay of oscillatory activity onset compared with channel 64. Asterisks in (D) and (F) indicate significantly higher cross-correlation (left) and coherence (right) values (*$p < 0.05$; ** $p < 0.01$; ***$p < 0.001$) from comparisons to channels 14 (D)

and 64 (F), respectively (z-test). CP, cortical plate; MZ, marginal zone; SP, subplate; WM, white matter. Picture from Sun and Luhmann, (2007).

Spontaneous network oscillations depend on gap junctional coupling

In order to study the role of gap junctions in the generation and propagation of spontaneous synchronized activity, the broad spectrum gap junction blocker carbenoxolone was bath applied at a concentration of 100 µM to neocortical slices showing spontaneous network oscillations. In four out of four slices tested (all from P0–P1 mice), carbenoxolone completely blocked the occurrence of spontaneous local as well as propagating synchronized network activity for observation periods of up to 1.5 h (Figure 17).

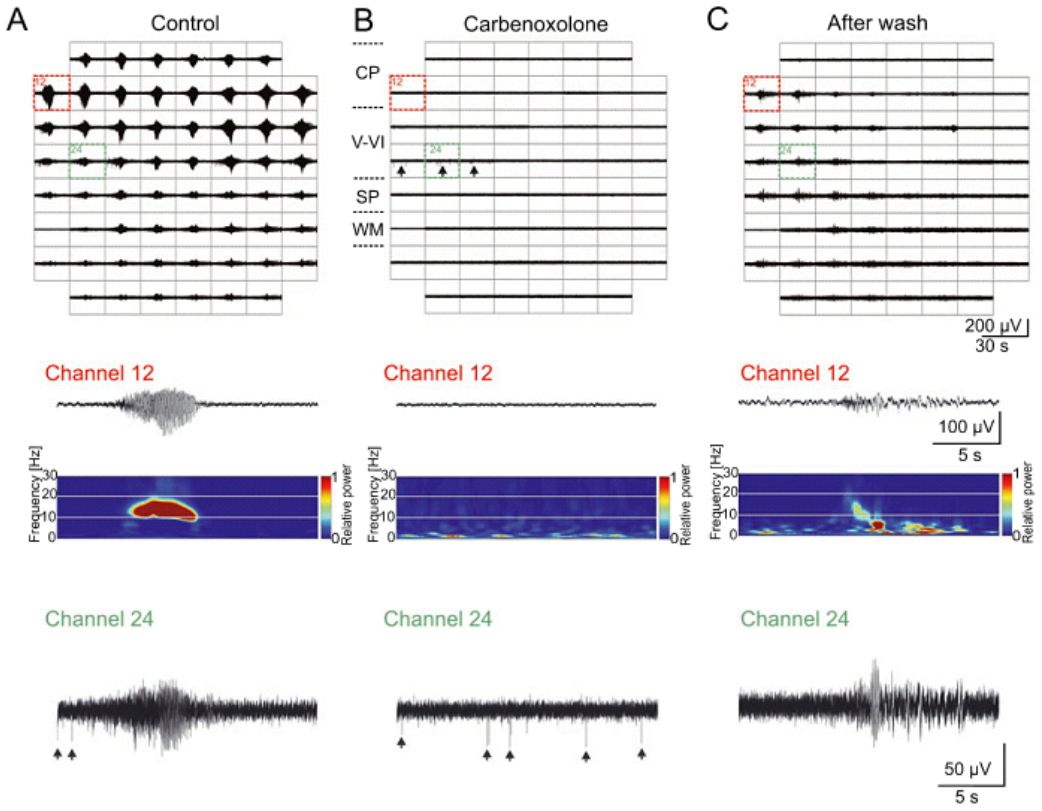

Figure 17. Spontaneous network oscillations require gap junctional coupling. (A), after addition of 100 µM carbenoxolone (B), and after 95 min washout of carbenoxolone (C). The middle panels show representative recordings obtained from channel 12 and corresponding wavelet analysis. During the 88-min application of carbenoxolone, no spontaneous network

oscillations could be recorded. However, non-synchronized spontaneous action potentials could be observed in carbenoxolone (arrows in MEA recordings in upper panel and in channel 24 recording in lower panel). CP, cortical plate; SP, subplate; WM, white matter. Picture from Sun and Luhmann, (2007).

Spontaneous activity partially recovered following carbenoxolone washout for 1–2 h (Figure 17C), demonstrating that gap junctions play an important role in the generation of synchronized oscillations in the newborn rodent cerebral cortex. Interestingly, spontaneous non-synchronized action potentials could be recorded in the presence of carbenoxolone (Figure 17B), demonstrating that spontaneous action potential firing was preserved but that carbenoxolone blocked the local synchronization of neuronal activity.

Electrical stimulation of the SP elicits oscillatory network activity

We have previously reported that the SP plays an important role in the generation of cholinergic network oscillations in the intact neocortex *in vitro* preparation of the newborn mouse (Dupont et al., 2006). Because the MEA chip allows a more detailed analysis of this SP-driven activity, we used a bipolar electrical stimulation protocol to activate the SP and to record the cortical network activity with a 200-µm MEA chip (Figure 18A). In all investigated slices (n=6), electrical stimulation of the SP elicited propagating oscillatory responses with an average peak frequency of 18 ± 1.5 Hz, duration of 0.6 ± 0.1 s and amplitude of 190.4 ± 41 µV (Figure 18B and C). These electrically evoked oscillations differ significantly in their duration and amplitude (both $p < 0.05$) from the spontaneous non-propagating activity and also in their peak frequency ($p < 0.001$) and duration ($p < 0.05$) from the spontaneous propagating oscillations.

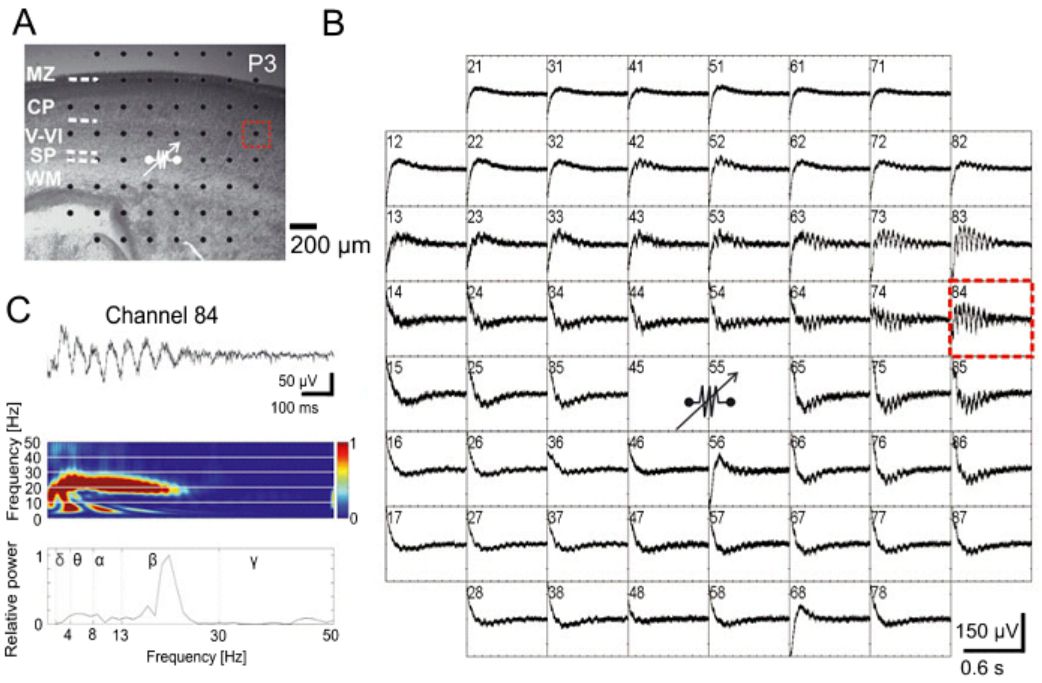

Figure 18. Local electrical stimulation of the subplate (SP) elicits propagating network oscillations. (A) Photograph of P3 mouse Nissl-stained coronal slice with cortical layers and position of MEA. (B) MEA recordings from the neocortical slice shown in (A), with the site of bipolar stimulation in the SP (80 µA, 200 µs duration, 50 Hz, 10 times). The spacing between the electrodes is 200 µm (see scale bar in A). (C) Recording at electrode number 84 (dotted red rectangle in A) shown at higher resolution with corresponding wavelet analysis and Fourier spectrum. CP, cortical plate; MZ, marginal zone; WM, white matter. Picture from Sun and Luhmann, (2007).

Cholinergic network oscillations

The spatio-temporal properties of cholinergic network oscillations in the newborn mouse somatosensory cortex were studied with MEA chips by bath application of the cholinergic agonist carbachol (30–100 µM). Whereas carbachol application to the intact cerebral cortex *in-vitro* preparation very reliably elicited oscillatory network oscillations activity in the newborn mouse (Dupont et al., 2006) and rat (Kilb and Luhmann, 2003), carbachol application to thick neocortical slices evoked the characteristic network response in only 36 out of 81 slices (44%; Figure 19). These oscillations showed an average frequency of 12.9 ± 0.7 Hz, duration of 9.3 ± 1.4 s and maximal amplitude of 161.0 ± 14.0 µV(n=35). These data further support our

hypothesis that an intact large neuronal network is required for the generation of network oscillations in the newborn rodent cerebral cortex.

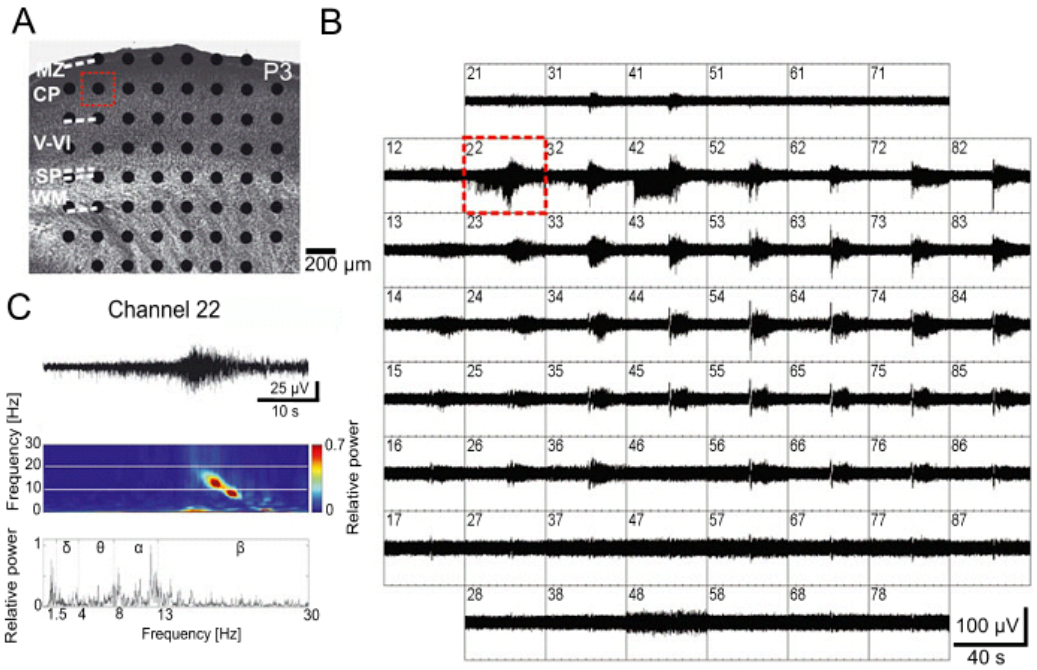

Figure 19. Carbachol-induced propagating network oscillations in the newborn mouse somatosensory cortex. (A) Photograph of a P3 mouse Nissl-stained coronal slice with cortical layers and position of MEA. (B) MEA recordings from the slice shown in (A) with carbachol (100 µM)-induced oscillatory network activity. The spacing between the electrodes is 200 µm (see scale bar in A). (C) Recording at electrode number 22 (dotted red rectangle in A) shown at higher resolution with corresponding wavelet analysis and Fourier spectrum. CP, cortical plate; MZ, marginal zone; SP, subplate; WM, white matter. Picture from Sun and Luhmann, (2007).

Neural activity in cultured neonatal mouse cerebral cortex

Further on, the small level of 350-µm thick brain slices from newborn mice was used. They were cultured over one week; the spatio-temporal properties of spontaneous neural activity and their pharmacological mechanisms on MEA were studied.

Electrophysiological characterization of spontaneous network activity in neocortical slice cultures

The organotypic slice culture was cultured onto a MEA system (Figure 20A), and the spontaneous neural activity was recorded with 60 extracellular electrodes with the MEA system. In agreement with previous *in vivo* and *in vitro* observations in newborn rodent cerebral cortex (Kilb and Luhmann, 2003;Khazipov et al., 2004;Dupont et al., 2006;Hanganu et al., 2006), neocortical slice cultures showed synchronized network oscillations. Spontaneous network oscillations could be recorded simultaneously over the whole MEA and in all cortical layers (Figure 20B). The spontaneous network oscillations occurred at an average interval of 6.7 ± 0.8 min (n = 8 slices) had a duration of 9.1 ± 0.65 s and a maximal amplitude of 679 ± 18 µV (n = 8 slices). Each event was characterized by an initial oscillation in the frequency range from 5 to 8 Hz, followed by repetitive wave-like discharges (Figure 20C). In 5 slice cultures, the activity appeared simultaneously at all recording sites, and in 9 slice cultures, the network oscillations propagated with an average velocity of 70.3 ± 4.9 mm/s over the MEA. Thus, the oscillatory activity in our neocortical slice cultures was highly correlated over a few hundred micrometers (Figure 20D and E).

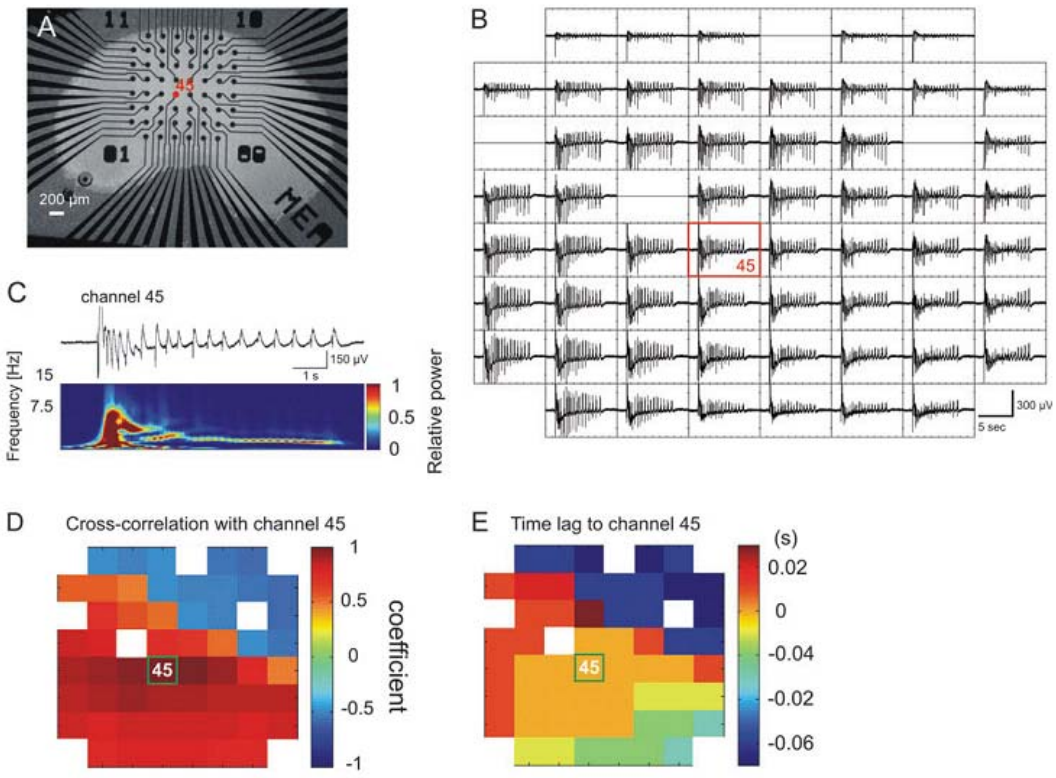

Figure 20. Synchronized spontaneous network activity in neocortical slice cultures. (A) Photograph of a 7 div organotypic neocortical slice culture placed on a 60-channel MEA. Black dots represent extracellular recording electrodes, separated by 200 µm. (B) Simultaneous 60-channel MEA recording from neocortical slice culture shown in (A). Four channels are damaged and were switched off. (C) Spontaneous oscillatory activity recorded with channel 45 and corresponding wavelet analysis. (D) Color plot illustrating the correlation coefficient calculated from cross-correlation analyses between channel 45 and all other channels. (E) Delay of activity onset recorded with channel 45 as compared with the activity onset in the other channels. Picture from Heck et al., (2008).

Activation of L-type Ca^{2+} channels

A selective N-methyl-D-aspartate (NMDA)-type receptor antagonist, 3-(2-Carboxypiperazin-4-yl) propyl-1-phosphonic acid (CPP), was used to investigate the activity pattern in CPP and high $[K^+]_e$. MEA multichannel recordings were performed from slices cultures treated with 10 µM CPP and 25 mM $[K^+]_e$ (Figure 21). Spontaneous events were completely blocked by CPP (n = 5 slices, Figure 21B). Upon addition of 25 mM extracellular potassium to the CPP-containing bathing

solution, a pronounced increase in activity with a maximal amplitude of 332 ± 97 µV could be observed (n = 3 slices, Figure 21C). However, this network activity with an average duration of 51.6 ± 16.2 s was observed only transiently during the washing phase of 25 mM potassium. Thereafter, no further network activity could be recorded for observation periods up to 1 hour.

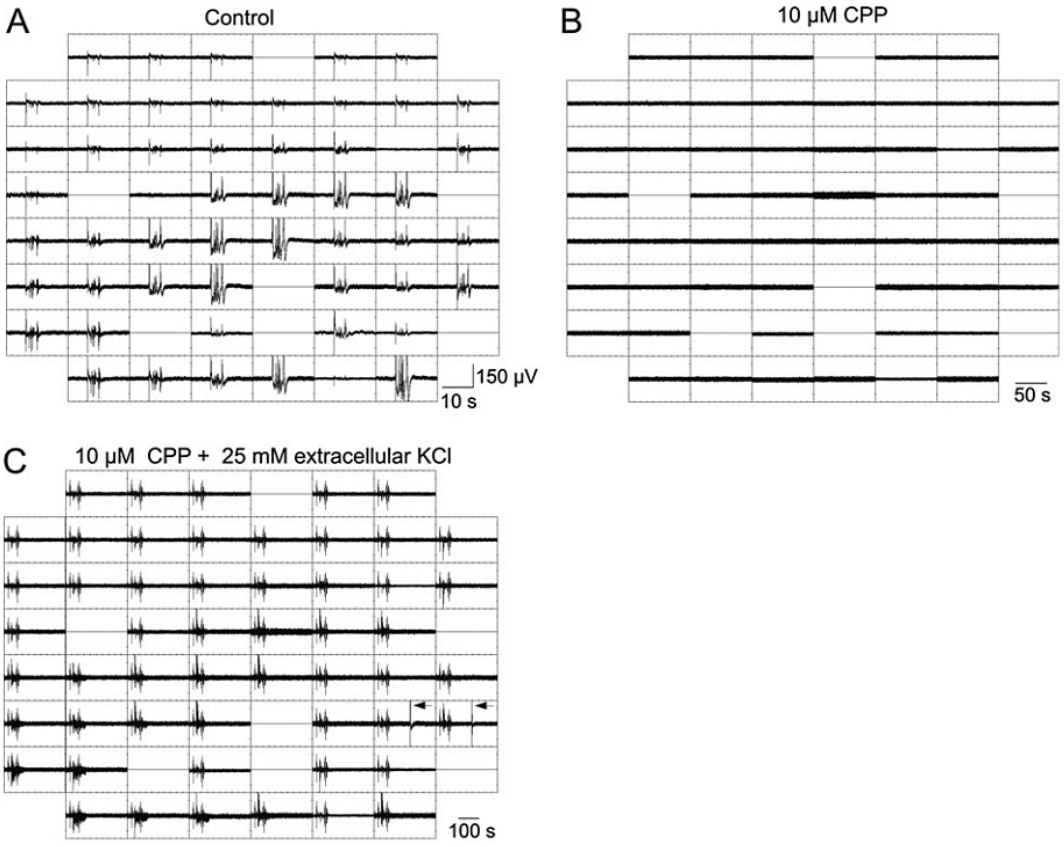

Figure 21. The effect of NMDA receptor antagonist CPP on spontaneous activity. (A-C) MEA recordings from the same 6 div slice cultures. Eight channels are damaged and were switched off. (A) Recordings in control condition reveal spontaneous and synchronized network bursts. (B) Spontaneous activity is blocked by the NMDA receptor antagonist CPP. (C) Addition of 25 mM potassium to the CPP containing ACSF causes a transient recovery in spontaneous network activity lasting 1.5 min. The arrows indicate that artifacts are present in 2 channels. Picture from Heck et al., (2008).

It has been demonstrated previously in neonatal mouse cerebral cortex that spontaneous, synchronous electrical activity could be blocked by the antagonist of L-type calcium channels nifedipine (Corlew et al., 2004b). The functional role of these voltage-dependent calcium channels on the network activity in neocortical slices cultures was studied by application of 10 µM nifedipine.

The NMDA receptor subunits NR2A and NR2B have different effects

To elucidate the contribution of different NMDA-R subunits in the NMDA-R-dependent spontaneous activity, we blocked the NR2A subunit with 400 nM NVP-AMM077 (Berberich et al., 2005) and the NR2B subunit with 3 µM ifenprodil (Williams, 1993). The NR2A subunit antagonist NVP-AMM077, a less effect on NR2B-type antagonist, induced a complete blockade of the spontaneous network activity recorded in normal extracellular solution (n = 3 slices, Figure 22A).

However, synchronous activity was observed in slices (n = 4) preincubated for 24 h in NVP-AMM077, which indicates that changes in the mechanisms that generate spontaneous activity occur to compensate for the blockade of NR2A-containing NMDA-R (data not shown). The NR2B subunit specific antagonist ifenprodil had no significant effect on the spontaneous network activity (Figure 22C). In addition, spontaneous activity was still present in slices (n = 2) preincubated for 24 h with ifenprodil (data not shown).

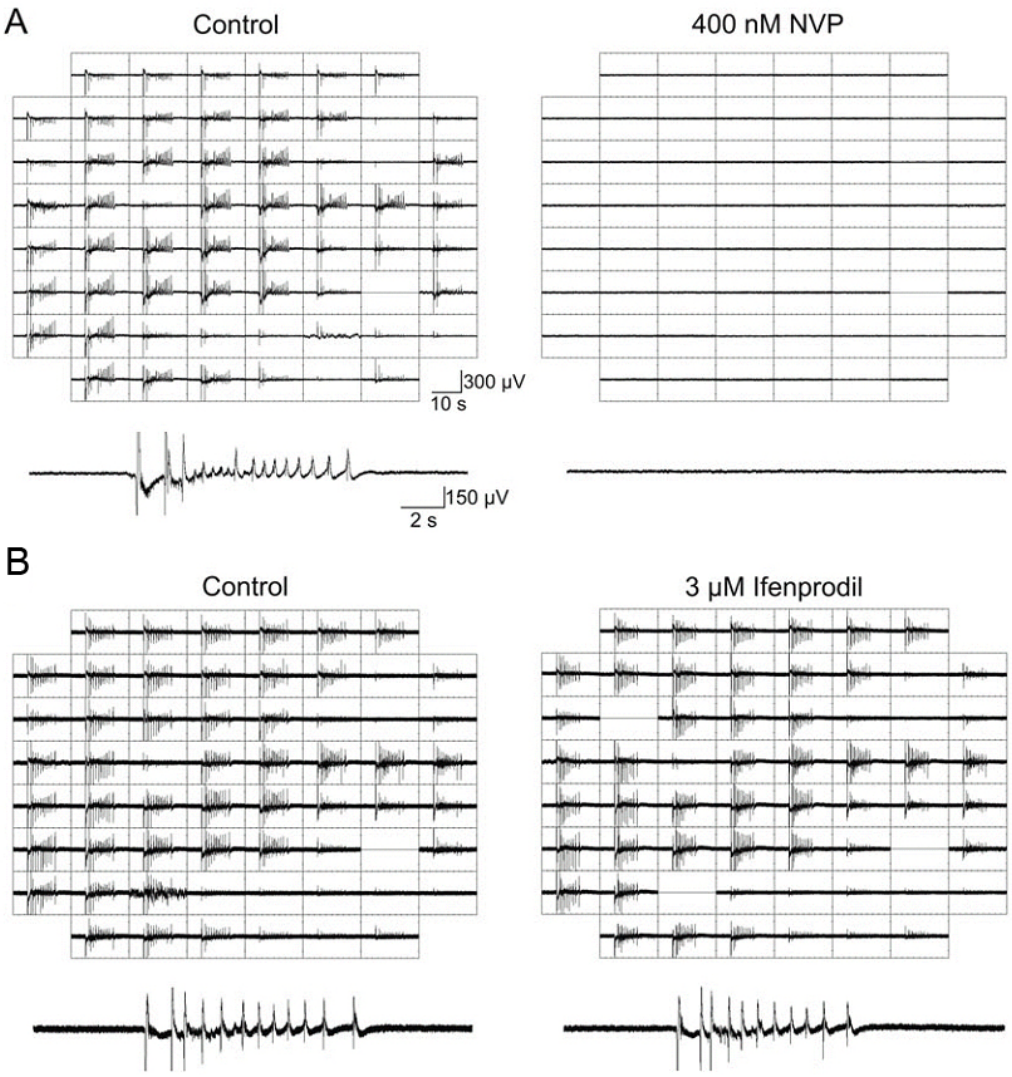

Figure 22. Blockade of NR2A-containing NMDA receptors leads to a complete loss of spontaneous activity. (A) Blockade of NR2A-containing NMD receptors with 400 nM NVP-AMM077 leads to a complete loss of spontaneous activity as recorded with the MEA system. (B) Blockade of NR2B-containing NMDA receptors with 3 µM ifenprodil does not change spontaneous network activity. Picture from Heck et al., (2008).

Role of GABA-A receptors in spontaneous network activity

The potential role of GABAergic synaptic mechanisms was also assessed. In control condition, spontaneous events recorded with the MEA system showed a pattern consisting of a prominent activity in the frequency range from 5 to 8 Hz (see Figure 23C and arrow in Figure 23A). After treatment with 100 µM gabazine, a specific antagonist of ionotropic gamma-aminobutyric acid (GABA) type A receptors, the amplitude of this activity was significantly reduced (control: 142.1 ± 13.4 µV; gabazine 36.9 ± 3.1 µV; $p < 0.0001$ Mann-Whitney test, 15 spontaneous events from n = 3 slices, Figure 23B).

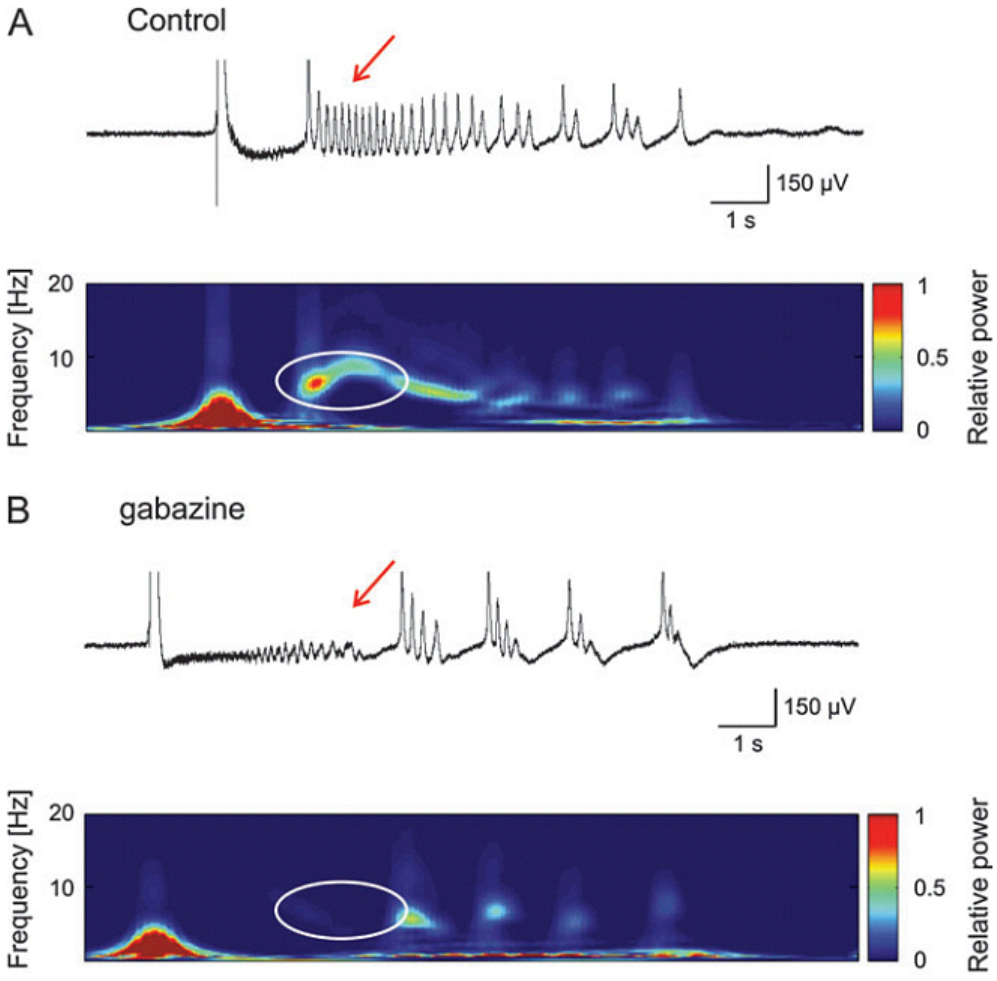

Figure 23. GABA receptor blockade causes suppression of spontaneous burst activity. (A) Representative extracellular field potential recording with the MEA system and corresponding color-coded wavelet analysis of a 6 div neocortical slice. (B) GABA-A

receptor blockade with 100 µM gabazine causes a reduction in the network activity, especially of the prominent activity in the 5 to 8 Hz frequency range (arrow and white ellipse in [A] and [B]). Picture from Heck et al., (2008).

Role of neuronal gap-junctions in spontaneous network activity

In agreement with previous observations in acute slice preparations from newborn rodents (Yuste et al., 1995;Kandler and Katz, 1998) and intact cortices (Dupont et al., 2006), synchronized network activity in neocortical slice cultures from newborn mice required intact gap junctional coupling. Application of 25 µM mefloquine, an inhibitor of neuronal, connexin 36-containing gap junctions (Cruikshank et al., 2004), blocked the synchronized network activity (n = 5 slices, Figure 24). Interestingly, the number of action potentials recorded extracellularly with the entire MEA in a 5-min observation period increased significantly ($p < 0.05$) from 31.5 ± 7.2 under control conditions to 138.1 ± 42.3 in mefloquine (n = 3 slices), indicating that spontaneous activity was still present, but no longer synchronized.

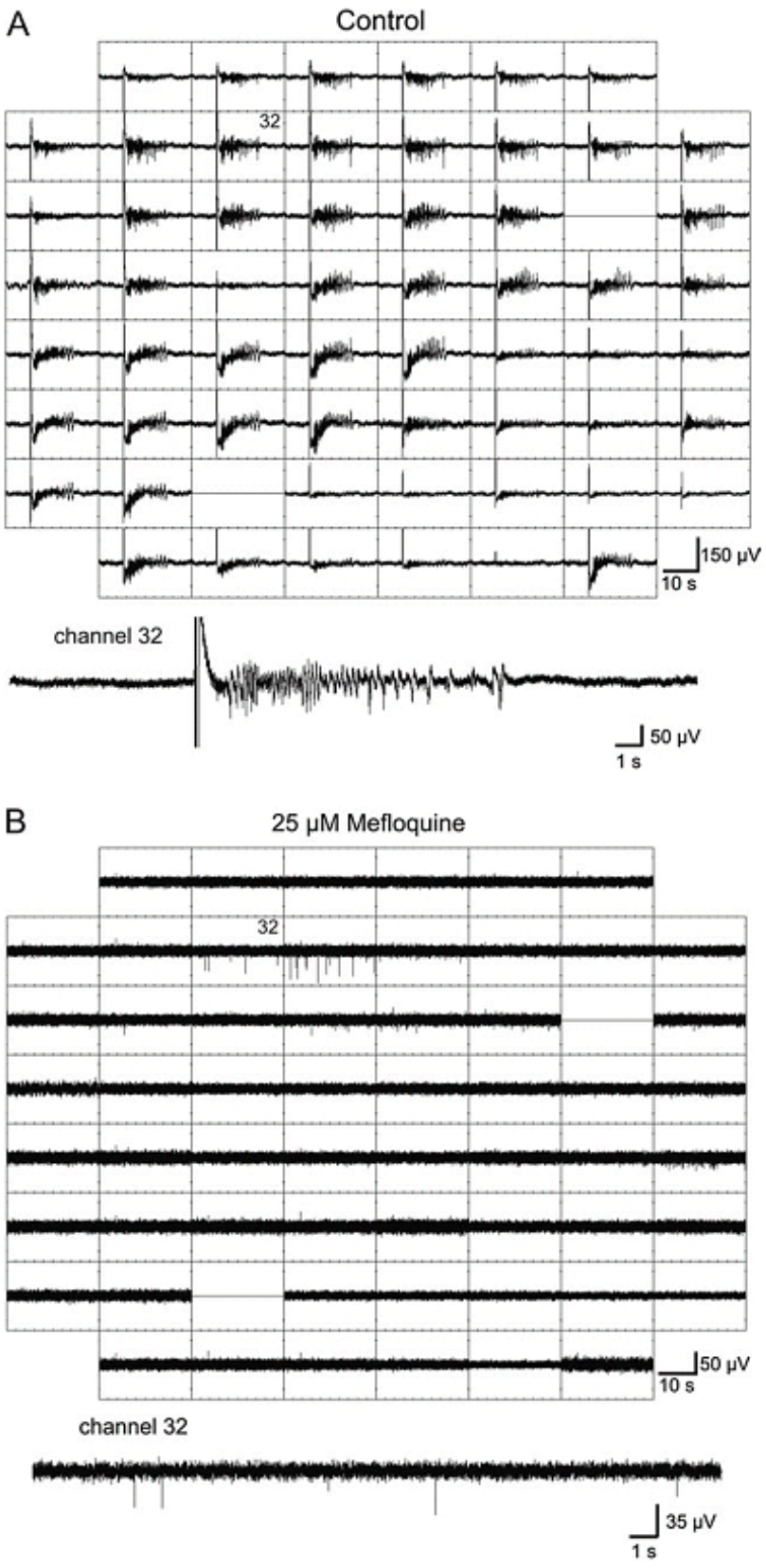
A
Control
32
150 µV
10 s
channel 32
50 µV
1 s
B
25 µM Mefloquine
32
50 µV
10 s
channel 32
35 µV
1 s

Figure 24. Effect of Gap junction blocker mefloquine on spontaneous burst activity. (A) MEA recordings under control conditions reveal large-scale spontaneous and synchronized network oscillations. (B) Bath application of the neuronal gap junction blocker mefloquine blocks synchronized network activity, but leaves spontaneous nonsynchronized action potential firing preserved. Picture from Heck et al., (2008).

Self-organization of recurrent spike patterns in developing neural networks *in vitro*

Underlying the spontaneous oscillations in acute slices and cultured slices, spike activity could be synchronized during oscillations (Ritz and Sejnowski, 1997). Oscillations act as background that brings neurons to the phase of synchronized depolarization (Nadasdy, 2000).These synchronized neurons are supposed to carry information according to Hebb's learning rules or cell assemble theory (see introduction; Hebb, 1949). Therefore, we used a cell culture model as well as template-matching algorithm (Abeles and Gerstein, 1988;Schrader et al., 2008) to investigate the emergence of repetitive spike patterns from mouse cortical neurons cultured on MEA.

Spontaneous activity during the development of cultured neural networks

We studied the development of spontaneous network activity of neocortical dissociated cell cultures (6 to 16 div) with 59-channel MEA. Datasets from ten different cultures were obtained under the same conditions. Spikes corresponding to individual neurons were separated from the dataset of detected spikes according to their characteristics of spike waveforms (see Figure 11 and Material and Methods). The average number of spiking neurons increased significantly from 2.3 ± 1.6 neurons per culture (n=9 cultures) at 6 div to 30 ± 5.5 neurons (n=10 cultures) at 15 div ($p < 0.0001$, ANOVA test; $p < 0.001$, followed by Dunnett post hoc test; Figure 25B). The mean firing rate showed a V-shape developmental profile, with higher mean firing rates at 6 div (0.24 ± 0.16 Hz, n=9 cultures) and at 15 div (0.20 ± 0.03 Hz, n=10 cultures). At 11 div, the neurons showed a comparative low mean firing rate (0.06 ± 0.01 Hz, n=10 cultures, Figure 25C).

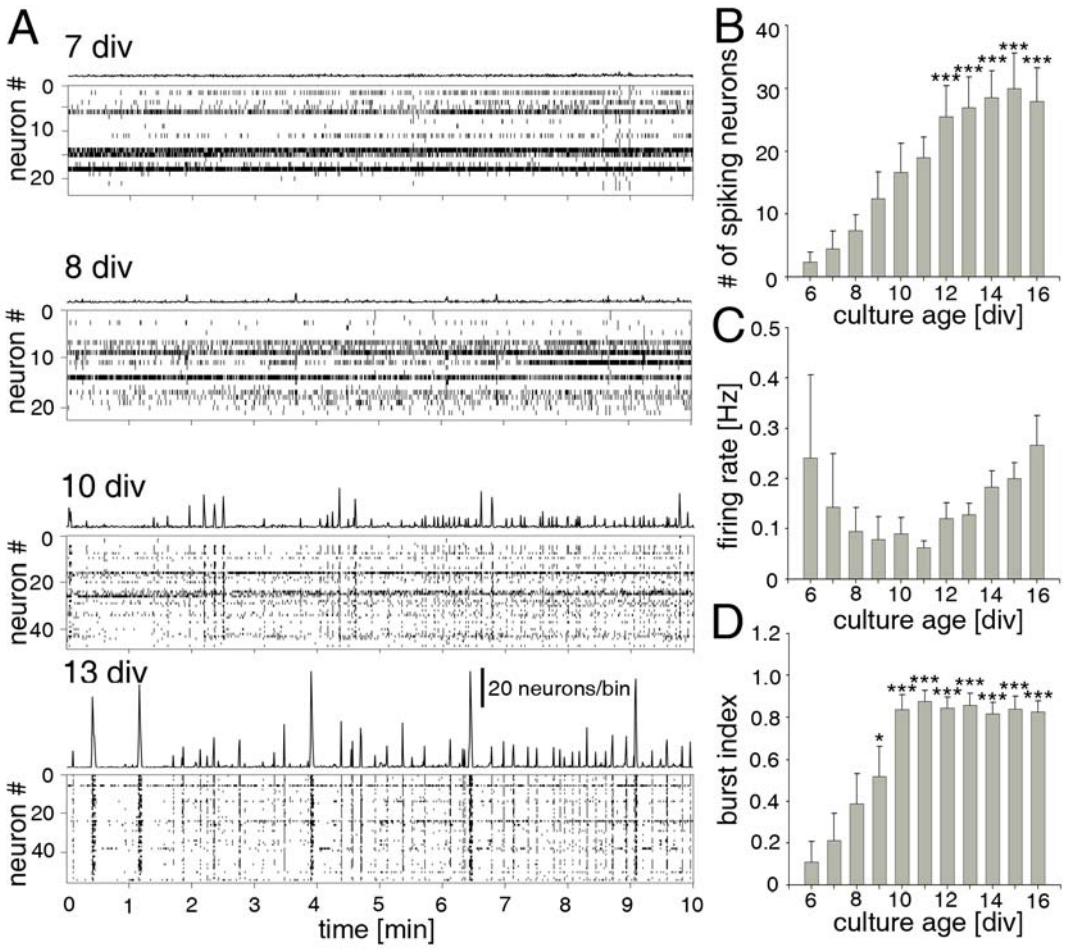

Figure 25. Spontaneous activity during the development of cultured neural networks. (A) Raster plot of activity (each dot presents a detected spike, lower part) and spike frequencies (upper part) in 0.6 s bins from 7, 8, 10 and 13 div for 10 minutes. Note that the bursts emerge at 8 div and become apparently at 13 div. Effects of age of cultures on the average number of spiking neurons (B), mean firing rate (spikes/neuron/sec) (C) and the temporal organization of the spikes, burst index (D), are quantified. The mean firing rate showed a V-shape developmental profile, with higher mean firing rates at 6 and 16 div. But at 11 div, the neurons presented a relative lower mean firing rate. One-way ANOVA test, $p < 0.0001$ in B and D; followed by Dunnett post hoc test versus 6 div; * $p < 0.05$; ***$p < 0.001$; n=10 cultures. Picture from Sun et al., (2009).

During this period, we observed the formation of recurrent synchronous bursting behavior, an example is shown in Figure 25A. The level of bursts was quantified by burst index (see Material and Methods), which increased from 0.11 ±

0.1 (n=9 cultures) at 6 div to 0.84 ± 0.06 (n=10 cultures) at 15 div (ANOVA test, $p < 0.0001$, followed by Dunnett post hoc test, $p < 0.001$) (Figure 25D).

Repetitive spike patterns during the development of cultured neural networks

The formations of recurrent bursts in culture neural networks were clearly shown previously (Figure 25A); furthermore, in order to investigate its underling assembly of neuronal connections, a template-matching algorithm (see Material and Methods) was used. Although there were several neurons at 6 or 7 div having high firing rates, surprisingly almost no repetitive spike patterns were detected at this age (n=6 cultures, i.e. Figure 26A 7 div). Starting at 8 div the repetitive spike patterns started to be identified and seen more and more frequent (Figure 26B, ANOVA test, $p < 0.01$, n=6 cultures). In addition, not only the average number of complexity (the number of the sequence) but also the average number of repetition of the repetitive spike patterns showed age-dependent increases (Figure 26C and D, n=6 cultures). On average we could identify a number of 28.8 ± 12.2 repetitive spike patterns (n=6 cultures, at 15 div), which had an average complexity of 5.4 ± 1.9 spikes and an average repetition of 3.1 ± 0.7 per 10 minutes. Further, we hypothesized that the appearances of repetitive spike patterns and recurrent bursts were correlated. The timings of recurrent bursts were identified by a burst detection algorithm (see Material and Methods) and the percentage of numbers of repetitive spike patterns appearing during these timings was calculated. The result, 94.2 ± 4.9 % (n=6 cultures, at 15 div) of the repetitive spike patterns appearing within the bursts, strongly supported our hypothesis.

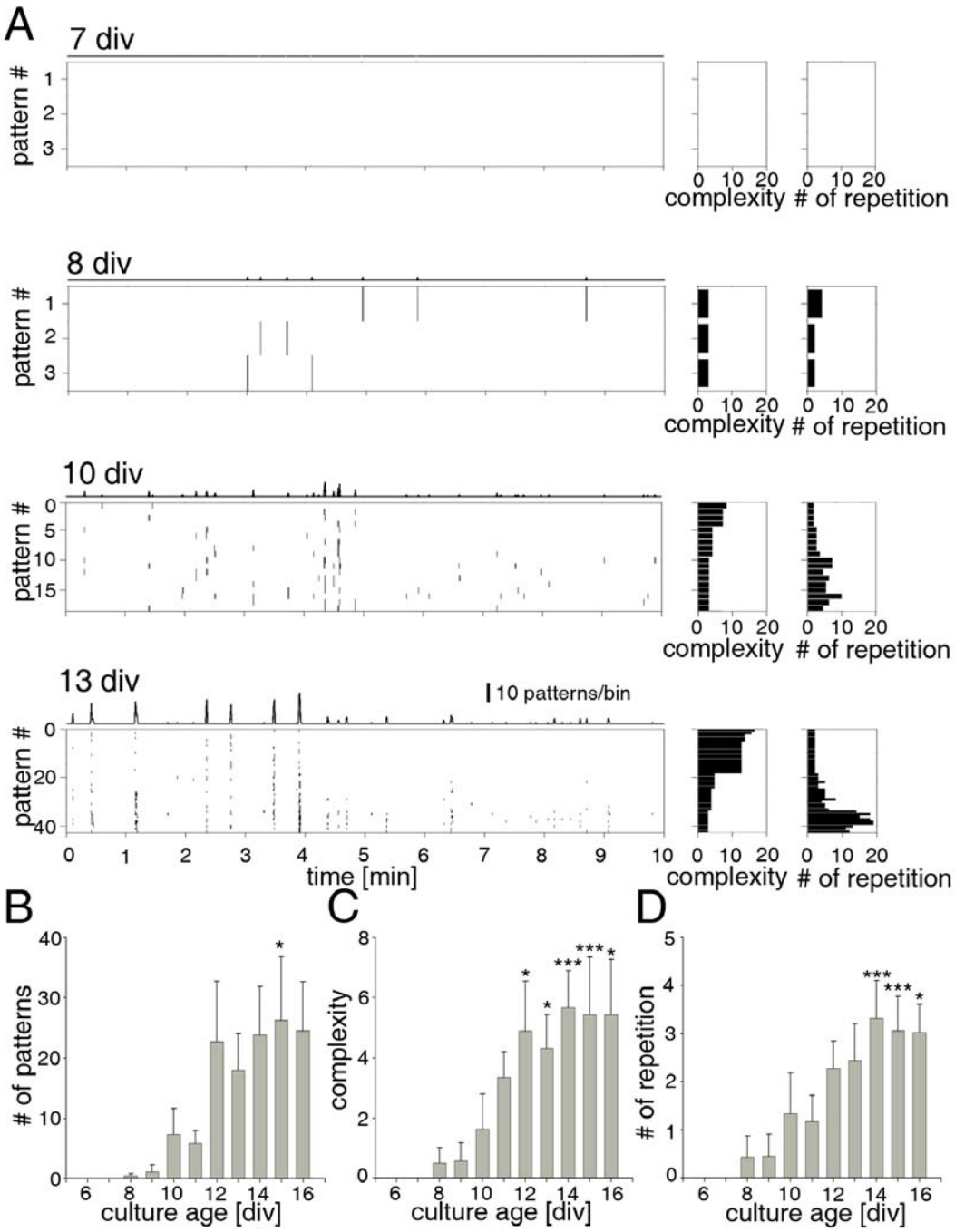

Figure 26. Repetitive spike patterns during the development of cultured neural networks. (A) Example of repetitive spike patterns at 7, 8, 10 and 13 div detected from the data shown in Figure 25A. The repetitions and complexity of individual repetitive spike patterns are shown on the right panels. Note that the average number (B), the average complexity (C) and the average number of repetition (D) of repetitive spike patterns showed age-dependent increases. One-way ANOVA test, $p < 0.01$ in B, C and D, and followed by

Dunnett post hoc test against 6 div; *$p < 0.05$; ***$p < 0.001$, n=6 cultures. Picture from Sun et al., (2009).

Hub neurons, lead neurons, stop neurons and functional connectivity

Hub neurons were identified by the definition of neurons having higher numbers of connections in neural networks than other neurons (see Material and Methods). The numbers of hub neurons, as well as their number of connections showed an age-dependent increase (Figure 27A and B, ANOVA test, $p < 0.01$, n=6 cultures). At 15 div, we obtained an average number off 5.7 ± 2.1 hub neurons (n=6 cultures, Figure 27A, Dunnett post hoc test, $p < 0.05$), which on average had 22.6 ± 12.3 connections.

Further, we showed the presence of particular neurons which are able to drive or stop the repetitive spike patterns. According to their functions we named them lead and stop neurons (see Material and Methods and Figure 14A). The numbers of lead and stop neurons also showed age-dependent increases (ANOVA test, $p < 0.01$, n=6 cultures). At 15 div, we obtained 2.2 ± 0.9 lead neurons and 1.3 ± 0.3 stop neurons (n=6 cultures, Figure 27C and D, Dunnett post hoc test, $p < 0.05$), in which each neuron on average participated to 6.2 ± 1.2 and 26.9 ± 19.8 repetitive spike patterns respectively.

In order to illustrate the neuronal circuits of cultured neural networks on MEA, the functional connectivity, which was based on the numbers of neuronal connections (see Material and Methods and Figure 14B), was applied. From 7 to 13 div, the numbers of neuronal connections showed an apparent increase; example maps of functional connectivity were illustrated in Figure 27E. It was clearly shown that the stronger connections occurred at 13 div and stable neuronal circuits were formed between hub neurons.

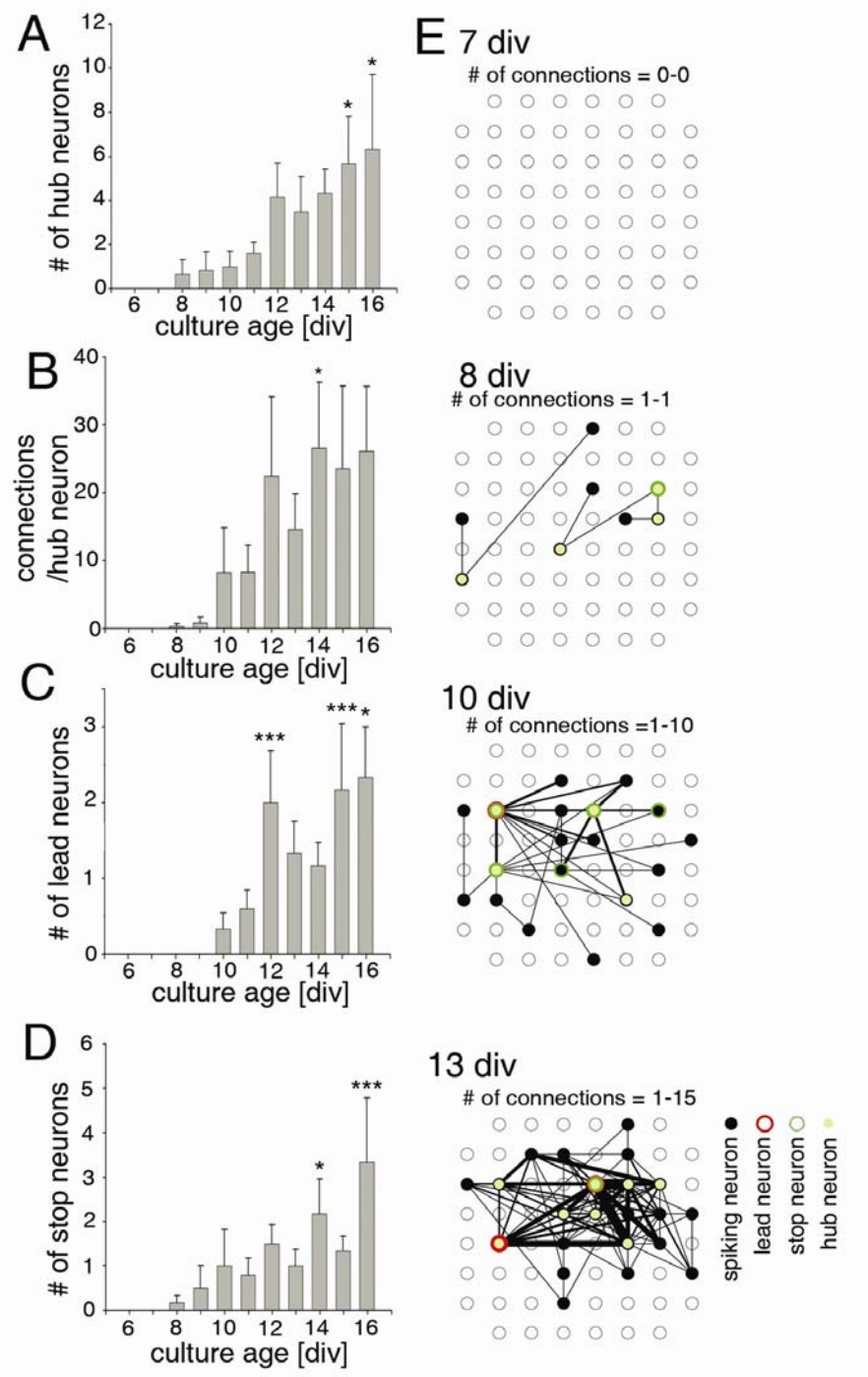

Figure 27. Hub neurons, lead neurons, stop neurons and functional connectivity in the development of cultured neural networks. The number of hub neurons (A), the average connections of hub neurons (B), the number of lead neurons (C) and the number of stop neurons (D) showe an age-dependent increase. These three types of neurons were identified by the appearing neurons in the repetitive spike patterns (see Material and Methods and Figure 14A) shown in Figure 26A. (E) The maps of functional connectivity are illustrated

based on the sequences of repetitive spike patterns (see Material and Methods and Figure 14B). The weight of lines indicates the total number of connections. Hub neurons, lead neurons and stop neurons are marked by different colors. One-way ANOVA test, $p < 0.001$ in A, B, C and D, and followed by Dunnett post hoc test against 6 div; *$p < 0.05$; ***$p < 0.001$, n=6 cultures. Picture from Sun et al., (2009).

Primary and merged patterns

A primary pattern (i.e. Fig. 28A) was defined as a repetitive spike pattern which appeared in many different repetitive spike patterns (see Material and Methods). Indeed, 41 out of 430 repetitive spike patterns (9.5 %, n=5 cultures, 10 to 16 div) were identified as primary patterns. They had an average complex of 3.3 ± 0.1 spikes (n=41 patterns from 5 cultures) and a relatively higher mean firing rate (9.3 ± 1.9 per 10 minutes, n=41 patterns from 5 cultures) compared to non-primary patterns (3.5 ± 0.5 per 10 minutes, $p < 0.01$, n=389 patterns from 5 cultures). On average one primary pattern participated in 3.3 ± 0.3 repetitive spike patterns. An example of primary pattern is shown in Fig. 28A, in which pattern 30, as a primary pattern, is involved in pattern 1 as well as in pattern 19.

In addition, we defined a merged pattern (i.e. Fig 28B) as a repetitive spike pattern which consisted of many different repetitive spike patterns (see Material and Methods). On average a merged pattern existed from 3.2 ± 0.3 repetitive spike patterns (n=30 from 4 cultures, 10 to 16 div), which had an average complex of 9.6 ± 1.2 spikes. An example of a merged pattern is shown in Fig. 28B, in which pattern 34 and pattern 20 merge together to be part of pattern 13.

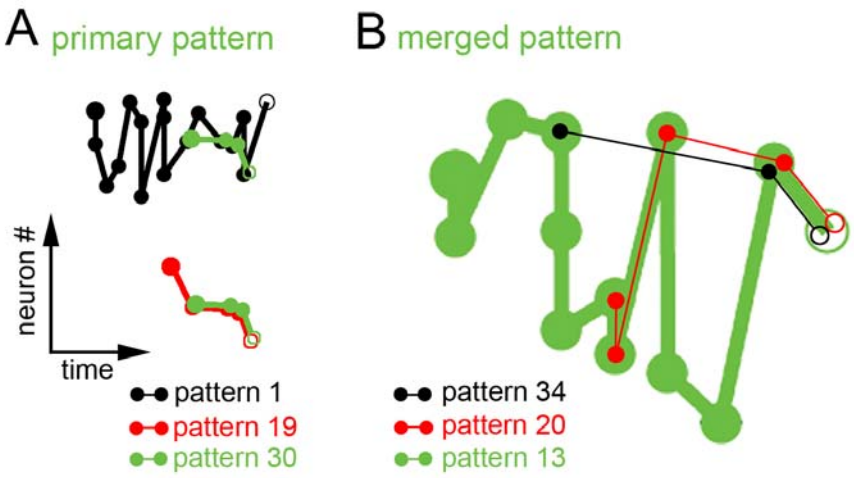

Figure 28. Primary patterns and merged patterns. (A) Three repetitive spike patterns are illustrated in spatio-temporal sequences, shown in Figure 26A (13 div). Pattern 30 (green) is defined as a primary pattern, which is involved in pattern 1 (black) as well as in pattern 19 (red). (B) Pattern 34 (black) and 20 (red) merged together to be part of pattern 13 (green), which is defined as a merged pattern. Via the z-test we examined the significance of the occurrence of primary patterns see Material and Methods). Picture from Sun et al., (2009).

5. Discussion

Spatio-temporal dynamics of oscillatory network activity in the acute neonatal mouse cerebral cortex

Using the 60-channel MEA chip we characterize with a high-temporal resolution the functional properties of oscillatory network activity in the newborn mouse somatosensory cortex *in vitro*. Our data clearly demonstrate that the probability of spontaneous network oscillations correlates with the thickness of the neocortical slices, strongly supporting the hypothesis that an intact neuronal network of sufficient dimension is required to generate this type of inherent activity. Wu and colleagues already showed that spontaneous hippocampal network rhythms do not consistently occur in conventional ~400-µm-thick slices with a limited network connectivity, but rather require an intact intrinsic circuitry that can only be maintained in slices with a thickness of ~1 mm (Wu et al., 2005a;Wu et al., 2005b). The spontaneous, carbachol- and stimulation-induced network oscillations described in the present study are in many aspects similar to those reported previously in the intact cerebral cortex *in vitro* preparation (Dupont et al., 2006), and the *in vivo* somatosensory or visual cortex of the newborn rat (Khazipov et al., 2004;Hanganu et al., 2006;Minlebaev et al., 2007). Spatially confined spindle-shaped field potential oscillations in the immature rat somatosensory and visual cortex show under *in vivo* conditions a similar frequency (10–20 Hz) and comparable duration as the local non-propagating spontaneous oscillations observed in the present study. However, *in vivo* spindle-shaped bursts occurred much more frequently in slightly older animals (2.5-8 per min; Khazipov et al., 2004;Hanganu et al., 2006;Minlebaev et al., 2007). This difference can be explained most likely by the fact that a large number of spindle bursts *in vivo* are triggered by the periphery (Khazipov et al., 2004;Hanganu et al., 2006), and that the rate of this spontaneous oscillatory activity increases significantly during the first postnatal days (Hanganu et al., 2006).

Propagating and non-propagating oscillatory activity

The use of the 60-channel MEA chip that covered a cortical area of 0.7 × 0.7 mm^2 (100 µm inter-electrode distance) or 1.4 × 1.4 mm^2 (200 µm inter-electrode distance) allowed us to differentiate between propagating and non-propagating synchronized network oscillations. Local non-propagating spontaneous oscillations with a high coherence could be recorded in a neocortical network of about 200 µm in diameter. Yuste et al. (1992) described so-called neuronal domains with similar spatial dimensions in neocortical slices from newborn rats by the use of fura-2 calcium imaging. They further demonstrated that the spontaneously coactive neurons within each neuronal domain are coupled by gap junctions. Our results are in good agreement with this previous report, and our electrophysiological recordings further demonstrate that neurons within these domains oscillate synchronously in the alpha/beta frequency range. It is tempting to speculate that these local oscillatory networks in the CP may represent an early functional template, a cortical 'precolumn', for the subsequent development of a cortical columnar network (Figure 15), e.g. a barrel in layer IV of the somatosensory cortex of rodents (Woolsey and Van der Loos, 1970). In the mouse, barrels can not be histologically identified with Nissl and cytochrome oxidase staining before P5 (Lee et al., 2005). However, our MEA recordings indicate that spontaneously active neurons form a functional neuronal network of ~200 µm in diameter already around birth. The question which mechanisms determine or influence the formation of this early neocortical network is currently not completely solved, but the 'radial unit hypothesis' certainly represents a good model (for review, see Rakic, 1988). Noctor et al. (2001) demonstrated that neocortical neurons migrate along clonally related radial glia, and suggests that the lineage relationship between neurons and proliferative radial glia may underlie the radial organization of the neocortex. It may well be that clonally related neurons in the developing cerebral cortex are initially coupled via gap junctions, which would also allow the exchange of biochemical signals (e.g. inositol trisphosphate;Kandler and Katz, 1998) and consolidation of connectivity patterns within an early neuronal ensemble. A number of recent studies demonstrated the presence of columnar, patterned, spontaneous activity in the immature cerebral cortex before the onset of the critical period, indicating that a columnar architecture develops earlier and more rapidly than was assumed previously (for review, see Katz and Crowley, 2002).

Not only neuroblasts are physiologically coupled by gap junctions into columnar clusters (LoTurco and Kriegstein, 1991), but also early generated SP neurons (Dupont et al., 2006). SP neurons are especially well suited to be activated during the earliest stages of cortical development by a thalamic input (Friauf et al., 1990;Hanganu et al., 2002;Higashi et al., 2002;Molnar et al., 2003) or by ascending neuromodulatory systems, such as the cholinergic projection (Calarco and Robertson, 1995;Mechawar and Descarries, 2001;Hanganu et al., 2007). During the early stages of corticogenesis, the SP functions as a reliable relay station between the various corticopetal inputs and the developing CP. The SP is required for the generation of cholinergic network oscillations in the neonatal mouse cerebral cortex (Dupont et al., 2006), and ablation of the SP at early stages prevents the formation of cortical columns (Dupont et al., 2006;Kanold, 2004). The present study demonstrates that electrical stimulation of the SP elicits oscillatory network activity that resembles in many aspects the spontaneous oscillations (Figure 18). This observation indicates that stimulation of the SP activates an intrinsic neocortical circuit, which is capable of generating this type of early synchronized activity.

Besides local non-propagating oscillations, a second type of spontaneous network activity could be observed in the large majority of the thick slice preparations. This activity propagated in the mediolateral or latero-medial direction over at least 1 mm and differed from the non-propagating oscillations in frequency, duration and amplitude. However, propagating spontaneous oscillations were also synchronized in a columnar manner, although in a larger network (Figure 16). This suggests that similar mechanisms mediate the functional coupling of local neuronal clusters in a propagating wave of activity. Spontaneous oscillations propagated in the horizontal direction with an average speed of 110 µm/s, which is very similar to the muscarine-induced traveling calcium waves described by Peinado (2000) in newborn rat neocortical slices (50–300 µm/s). The significant faster propagation speed in the vertical direction (2.4 ± mm/s) compared with the horizontal direction (0.11 mm/s) may result from a higher columnar coupling efficiency. Interestingly, a faster intracortical spread of activity in the vertical direction could also be observed by the use of optical recording techniques in adult neocortical slices (Abeles and Gerstein, 1988). Calcium imaging studies (Yuste et al., 1992;Kandler and Katz, 1998) as well as dye coupling experiments (LoTurco and Kriegstein, 1991;Dupont et al., 2006) in

neocortical slices from neonatal rodents have previously documented a columnar organization of electrically coupled neurons, suggesting a more efficient coupling in the vertical direction.

Why should the neonatal cerebral cortex oscillate?

Synchronized oscillatory activity represents a common functional property of many immature neuronal networks (see *Introduction*, and Moody and Bosma, 2005). In the cerebral cortex, early network oscillations can be either generated spontaneously (Garaschuk et al., 2000;Opitz et al., 2002;McCabe et al., 2006;Minlebaev et al., 2007;Sun and Luhmann, 2007), driven by the periphery (Khazipov et al., 2004;Hanganu et al., 2006;Minlebaev et al., 2007) or elicited by ascending neuromodulatory inputs (Hanganu et al., 2007). Rapid oscillatory activity in the alpha/beta frequency range has not only been observed in the cerebral cortex of newborn animals, but also in the neocortex of premature human neonates of 29–31 weeks post-conceptional age (Vanhatalo et al., 2005;Milh et al., 2007); (for review, see Khazipov and Luhmann, 2006). Synchronized network oscillations in the alpha/beta frequency range may reflect an intrinsic capacity of the immature cerebral cortex to generate early functional networks. Perturbations of this early activity, like disruption of the spontaneous input from the retina before the onset of vision, results in a structural and functional disorganization of the columnar architecture and in imprecise maps in the primary visual cortex (Cang et al., 2005;Huberman et al., 2006). Activity patterns during this so-called 'precritical period' would enable the formation of early networks and maps, which are subsequently fine-tuned during the critical period by experience-dependent mechanisms (for review, see Feller and Scanziani, 2005).

The mature cortex generates a variety of oscillatory activities that play a central role in different physiological and pathophysiological processes (for comprehensive review, see Buzsáki, 2006). Approximately once every 3–5 sec the adult cerebral cortex reveals a rhythmic pattern of activity, which is generated by intracortical recurrent excitation and regulated by synaptic inhibition (so-called 'UP' or depolarized state; Sanchez-Vives and McCormick, 2000). This intrinsic activity pattern can be observed in the mature cortex *in vivo* (for review, see Destexhe et al., 2003), as well as in neocortical slices when the bath solution resembles the *in vivo* situation in its ionic composition (e.g. 1mM Ca^{2+} ,1mm Mg^{2+} , 3.5 mm K^{+}) (Sanchez-

Vives and McCormick, 2000). However, these recurrent depolarizations occur less frequently in neocortical slices from immature animals (Tseng and O'Donnell, 2005), especially when the slices are relatively thin (300 µm). The functional role of oscillatory network activity in the pre- and neonatal cortex is currently not clear. It has been suggested that certain temporal patterns of electrical activity and intracellular calcium signaling may play specific roles in the activity-dependent regulation of gene expression, and the other way round that specific genes are regulated by specific patterns of activity (for review, see Fields et al., 2005;Torborg and Feller, 2005). Two recent reports have demonstrated that the periodic spontaneous activity pattern of retinal ganglion cells is correlated with activation of the cAMP pathway, which is needed for establishing the retinotopic map (Dunn et al., 2006;Nicol et al., 2007). Retinal ganglion cells must fire high-frequency bursts with a slow periodicity on a timescale of seconds to minutes to activate the intracellular biochemical cascade. Repetitive burst discharges also represent the ideal stimulus pattern for the secretion of brain-derived neurotrophic factor (for review, see Lessmann et al., 2003), which plays a central role as survival factor and is important for the activity-dependent formation of early neuronal networks (for review, see Huang and Reichardt, 2001). Early oscillatory activity may not only control progressive processes as network formation, but also regressive processes, such as the activity-dependent regulation of programmed cell death in the developing cerebral cortex (Heck et al., 2008). It remains to be elucidated which electrical activity patterns and which molecular mechanisms regulate the formation of neuronal networks during early stages of corticogenesis.

Neural activity in organotypic slice cultures of the neonatal mouse cerebral cortex

The main conclusions of our study regarding the role of electrical activity in organotypic slice cultures of the neonatal mouse somatosensory cortex can be summarized as follows: (1) Synchronized spontaneous network activity was observed in neocortical slice cultures. (2) NMDA-R containing the NR2A or NR2B subunit show a different acute effect on the neural activity. (3) The inhibition of ionotropic

GABA receptors induced a change in spontaneous activity. (4) Gap-junctional coupling modulates spontaneous network activity.

Our data demonstrate that spontaneous neunal activity, mediated by glutamatergic synapses and by neuronal gap junctions, plays an important role in the developing cerebral cortex. Since the spontaneous electrical activity recorded in organotypic neocortical slice cultures resembles in many aspects the spontaneous activity patterns observed *in vivo*, our observations are probably also relevant during early cortical development *in vivo*.

Pharmacological modulation on spontaneous oscillations

The pattern of spontaneous neural activity recorded at the network level with MEA resembled the *in vivo* activity pattern observed in the rodent cerebral cortex during the first postnatal week (Khazipov et al., 2004;Hanganu et al., 2006) (for review, see Khazipov and Luhmann, 2006;Moody and Bosma, 2005). Spontaneous TTX-sensitive bursts and synchronized network activity could be blocked by ionotropic glutamate receptor antagonists (Minlebaev et al., 2007) and during earlier developmental stage with gap junction blockers ((Yuste et al., 1992;Dupont et al., 2006). The cultured brain slice model confirmes again the role of gap junctions in development of cortex that, described previously in "*propagating and non-propagating oscillatory activity"* section of discussion. Gap junctions allow the exchange of biochemical signals (i.e. inositol trisphosphate; Kandler and Katz, 1998) and consolidation of connectivity patterns within an early neuronal ensemble.

Dupont (2006) has shown that the synchronized network activity from young animals (P5–P7) was completely blocked by NMDA receptor antagonist, CPP. Our data is in line with this conclusion; furthermore we provided data that suggest the NR2A-containing NMDA receptors are responsible for the early neocortical network activity (Figure 22). Nevertheless, blockade of NR2B-containing NMDA receptors with ifenprodil does not change spontaneous network activity (Figure 22). Our data also illustrated that under blockade of NMDA-R, an increase in $[K^+]_e$ elicited a transient synchronized network activity (Figure 21). Although calcium influx via NMDA-Rs and L-type calcium channels activate different calcium binding proteins (Marshall et al., 2003b), both pathways activate kinases leading to CREB dependent BDNF synthesis (Ghosh et al., 1994;Dolmetsch et al., 2001). Interestingly, Ca^{2+}-

influx via NMDA-Rs or L-type voltage gated calcium channels are the two key mechanisms to elicit activity-dependent release of BDNF and NT-3 in central neuronal cultures (Kolarow et al., 2007).

Moreover, the inhibition of GABA receptors with gabazize induced a change in the activity pattern with the loss of the prominent 5–8 Hz component (Figure 23). It is tempting to speculate that gabazine reduces the excitatory GABAergic synapses (for review, see Cossart et al., 2005) and results in the consequent reduction of the 5-8 Hz frequency band. It has been previously reported that burst activity, rather than a steady rate of single action potentials is more effective in triggering BDNF release (Hartmann et al., 2001;Balkowiec and Katz, 2002). This suggests that activity-dependent release of BDNF (Kuczewski et al., 2008) (for review, see Lessmann et al., 2003) could account for the activity-dependent neuronal development in our cultures.

Self-organization of recurrent spike patterns in developing neural networks *in vitro*

The main results are as follows. (1) The numbers of spiking neurons increase dramatically between 6 to 16 div as well as the burst index. (2) Repetitive spike patterns emerge after one week of culture and dramatically increase their numbers as well as their complexity and occurrence in the second week. (3) The hub neurons dominate the neural network, and their numbers of connections increase apparently. (4) Particular repetitive spike patterns, which are strongly interconnected, may serve as basal units for other patterns. Different repetitive spike patterns can merge together and generate another more complex pattern.

Internally generated repetitive spike patterns

One week after plating dissociated neurons on MEA, we observed a large variability of autonomous spontaneous activities from spiking neurons. At the end of the second week in culture, the activity can be temporally correlated, showing synchronous bursts behavior. Within the bursts, neurons show non-randomly distributed repetitive spike patterns, which have significant higher repetitions than surrogates. These precisely tempo-spatial repetitive spike patterns indicate that neural networks on

MEA not only can sustain spontaneous activities, but that they are capable of generating temporal relations between spikes. Moreover, these repetitive spike patterns imply that many microcircuits exist in the neuronal culture on the MEA. We conclude that dissociated neurons can self-organize themselves in neural networks and can emerge a number of dynamic repetitive spike patterns. This result is in line with a number of previous studies (Segev et al., 2004;van Pelt et al., 2004;Rolston et al., 2007;Baruchi et al., 2008;Pasquale et al., 2008).

Despite the large variability of repetitive spike patterns found, we successfully identified certain repetitive spike patterns, defined as "primary patterns", which emerge at a higher frequency and play a role as basal units. It is tempting to speculate that some neurons are strongly interconnected with each other, form more rigid microcircuits, and may therefore serve as basal units for other patterns. On the other hand, we also found that two or more repetitive spike patterns can merge together into another more complex pattern. Thus, these data suggest that information processing and storage in neural networks may be based on basal units generating repetitive spike patterns.

Mechanisms of repetitive spike patterns

Several hypotheses have been purposed for the mechanisms of repetitive spike patterns: Hebb learning rules (1949), spike-time dependent synaptic plasticity (STDP, Zhang et al., 1998;Bi and Poo, 1998) and intrinsic "pacemaker" cells. The Hebbian rule may explain the formation of neuronal connections, saying "when an axon of cell A is near enough to excite a cell B and repeatedly or persistently takes part in firing it, some growth process or metabolic change takes place in one or both cells such that A's efficiency, as one of the cell firing B, in increased." He suggested that individual neurons could participate in different cell assemblies and be involved in multiple functions and representations. His speculation is exactly in line with our observation of "primary patterns", which have stable representation and are involved in many cell assemblies. The theory of STDP provides a more detailed explanation, saying "synapses strengthen when presynaptic firing precedes postsynaptic firing but weaken when the sequence is reversed." This "plasticity" mechanism may tune the connections of neural network. Until now, there is still need to clarify the role of STDP on cell assembly of living neurons.

Neuronal cultures have been proved to be scale-free networks, which have a power-law function for the firing rate (Eytan and Marom, 2006) as well as the size and duration of neuronal avalanches (Pasquale et al., 2008). In our study, this neural network is dominated by a number of hub neurons, which are identified by their relative high connectivity and may serve as "pacemaker" cells. Moreover, some neurons, which can drive repetitive spike patterns, were found in evoked and spontaneous bursts (Eytan and Marom, 2006). of The lead neurons in our data supports this finding.

Repetitive spike patterns in brain slices and in vivo

As mentioned previously, repetitive spike patterns have been found in brain slices as well as in vivo, both have an intact structure. In these two systems, the repetitive spike patterns could emerge spontaneously or by external stimulation. Using calcium imaging of mouse thalamocortical slices, MacLean and colleagues demonstrated that the spatio-temporal patterns occur in spontaneous network events and trigger thalamically network activities (MacLean et al., 2005). Moreover, both network activities shared the same cell assemblies and showed comparable spatio-temporal properties.

A number of in vivo studies have shown that repetitive spike patterns are related to different brain functions. Repetitive spike patterns in the hippocampus may change their sequences by learning and could be replayed during sleeping (Nadasdy et al., 1999). In the prefrontal cortex, the monosynaptic interaction between pairs of assembled neurons changed during a working memory task (Fujisawa et al., 2008). In sensory systems, external stimulation such as tactile stimuli (Nicolelis et al., 1997) or order stimuli (Wehr and Laurent, 1996), could elicit unique spatio-temporal patterns of neuron firing. In motor cortex, it has been shown that neuronal ensembles are represented in a number of similar motion task (Abeles et al., 1995).

In conclusion, our findings demonstrate that dissociated neurons can self-organize themselves, assemble in a neural network, and emerge spatio-temporal activation patterns. The repetitive spike patterns implicate particular cell assemblies, which may serve a fundamental function for information processing and storage in the brain.

6. Summary

Information processing and storage in the brain may be presented by the oscillations and cell assemblies. Here we address the question of how individual neurons associate together to assemble neural networks and present spontaneous electrical activity. Therefore, we dissected the neonatal brain at three different levels: acute 1-mm thick brain slice, cultured organotypic 350-µm thick brain slice and dissociated neuronal cultures. The spatio-temporal properties of neural activity were investigated by using a 60-channel Micro-electrode arrays (MEA), and the cell assemblies were studied by using a template-matching method. We find local on-propagating as well as large-scale propagating spontaneous oscillatory activity in acute slices, spontaneous network activity characterized by synchronized burst discharges in organotypic cultured slices, and autonomous bursting behaviour in dissociated neuronal cultures. Furthermore, repetitive spike patterns emerge after one week of dissociated neuronal culture and dramatically increase their numbers as well as their complexity and occurrence in the second week. Our data indicate that neurons can self-organize themselves, assembly to a neural network, present spontaneous oscillations, and emerge spatio-temporal activation patterns. The spontaneous oscillations and repetitive spike patterns may serve fundamental functions for information processing and storage in the brain.

Reference list

Abeles M, Bergman H, Gat I, Meilijson I, Seidemann E, Tishby N, Vaadia E (1995) Cortical Activity Flips Among Quasi-Stationary States. Proc Natl Acad Sci USA 92:8616-8620.

Abeles M, Gerstein GL (1988) Detecting spatiotemporal firing patterns among simultaneously recorded single neurons. J Neurophysiol 60:909-924.

Allendoerfer KL, Shatz CJ (1994) The subplate, a transient neocortical structure: Its role in the development of connections between thalamus and cortex. Annu Rev Neurosci 17:185-218.

Ascoli GA, et al. (2008) Petilla terminology: nomenclature of features of GABAergic interneurons of the cerebral cortex. Nat Rev Neurosci 9:557-568.

Balkowiec A, Katz DM (2002) Cellular mechanisms regulating activity-dependent release of native brain-derived neurotrophic factor from hippocampal neurons. J Neurosci 22:10399-10407.

Baruchi I, Volman V, Raichman N, Shein M, Ben Jacob E (2008) The emergence and properties of mutual synchronization in in vitro coupled cortical networks. Eur J Neurosci 28:1825-1835.

Berberich S, Punnakkal P, Jensen V, Pawlak V, Seeburg PH, Hvalby O, Kohr G (2005) Lack of NMDA receptor subtype selectivity for hippocampal long-term potentiation. J Neurosci 25:6907-6910.

Berger H (1929) Ueber das Elektroenkephalogramm des Menschen. Archiv fuer Psychiatrie und Nervenkrankheiten 87:527-570.

Bi GQ, Poo MM (1998) Synaptic modifications in cultured hippocampal neurons: Dependence on spike timing, synaptic strength, and postsynaptic cell type. Journal of Neuroscience 18:10464-10472.

Blanche TJ, Spacek MA, Hetke JF, Swindale NV (2005) Polytrodes: high-density silicon electrode arrays for large-scale multiunit recording. J Neurophysiol 93:2987-3000.

Bloom FE, McConnell SK, Roberts JL, Spitzer NC, Zigmund MJ (2002) Fundamental Neuroscience (CD-ROM). Academic Press Inc , USA.

Buzsáki G (2006) Rhythms of the brain. Oxford University Express.

Buzsaki G, Chrobak JJ (1995) Temporal Structure in Spatially Organized Neuronal Ensembles - A Role for Interneuronal Networks. Curr Opin Neurobiol 5:504-510.

Buzsáki G, Chrobak JJ (1995) Temporal structure in spatially organized neuronal ensembles: A role for interneuronal networks. Curr Opin Neurobiol 5:504-510.

Buzsaki G, Draguhn A (2004) Neuronal oscillations in cortical networks. Science 304:1926-1929.

Calarco CA, Robertson RT (1995) Development of basal forebrain projections to visual cortex: DiI studies in rat. J Comp Neurol 354:608-626.

Calderon DP, Leverkova N, Peinado A (2005) Gq/11-induced and spontaneous waves of coordinated network activation in developing frontal cortex. J Neurosci 25:1737-1749.

Cang J, Renteria RC, Kaneko M, Liu X, Copenhagen DR, Stryker MP (2005) Development of precise maps in visual cortex requires patterned spontaneous activity in the retina. Neuron 48:797-809.

Caton R (1875) The electric currents of the brain. Br Med J 2:278.

Corlew R, Bosma MM, Moody WJ (2004b) Spontaneous, synchronous electrical activity in neonatal mouse cortical neurons. J Physiol 560:377-390.

Corlew R, Bosma MM, Moody WJ (2004a) Spontaneous, synchronous electrical activity in neonatal mouse cortical neurons. J Physiol 560:377-390.

Cossart R, Bernard C, Ben-Ari Y (2005) Multiple facets of GABAergic neurons and synapses: multiple fates of GABA signalling in epilepsies. Trends Neurosci 28:108-115.

Cruikshank SJ, Hopperstad M, Younger M, Connors BW, Spray DC, Srinivas M (2004) Potent block of Cx36 and Cx50 gap junction channels by mefloquine. Proc Natl Acad Sci U S A 101:12364-12369.

Destexhe A, Rudolph M, Paré D (2003) The high-conductance state of neocortical neurons in vivo. Nat Rev Neurosci 4:739-751.

Dolmetsch RE, Pajvani U, Fife K, Spotts JM, Greenberg ME (2001) Signaling to the nucleus by an L-type calcium channel - Calmodulin complex through the MAP kinase pathway. Science 294:333-339.

Droge MH, Gross GW, Hightower MH, Czisny LE (1986) Multielectrode analysis of coordinated, multisite, rhythmic bursting in cultured CNS monolayer networks. J Neurosci 6:1583-1592.

Dunn TA, Wang CT, Colicos MA, Zaccolo M, DiPilato LM, Zhang J, Tsien RY, Feller MB (2006) Imaging of cAMP levels and protein kinase A activity reveals that retinal waves drive oscillations in second-messenger cascades. J Neurosci 26:12807-12815.

Dupont E, Hanganu IL, Kilb W, Hirsch S, Luhmann HJ (2006) Rapid developmental switch in the mechanisms driving early cortical columnar networks. Nature 439:79-83.

Elias LA, Kriegstein AR (2008) Gap junctions: multifaceted regulators of embryonic cortical development. Trends Neurosci 31:243-250.

Elias LA, Wang DD, Kriegstein AR (2007) Gap junction adhesion is necessary for radial migration in the neocortex. Nature 448:901-907.

Engel AK, Fries P, Singer W (2001) Dynamic predictions: Oscillations and synchrony in top-down processing. Nat Rev Neurosci 2:704-716.

Eytan D, Marom S (2006) Dynamics and effective topology underlying synchronization in networks of cortical neurons. J Neurosci 26:8465-8476.

Farber K, Kettenmann H (2005) Physiology of microglial cells. Brain Res Rev 48:133-143.

Feller MB, Scanziani M (2005) A precritical period for plasticity in visual cortex. Curr Opin Neurobiol 15:94-100.

Fields RD, Lee PR, Cohen JE (2005) Temporal integration of intracellular Ca2+ signaling networks in regulating gene expression by action potentials. Cell Calcium 37:433-442.

Firth SI, Wang CT, Feller MB (2005) Retinal waves: mechanisms and function in visual system development. Cell Calcium 37:425-432.

Flint AC, Dammerman RS, Kriegstein AR (1999) Endogenous activation of metabotropic glutamate receptors in neocortical development causes neuronal calcium oscillations. Proc Natl Acad Sci USA 96:12144-12149.

Friauf E, McConnell SK, Shatz CJ (1990) Functional synaptic circuits in the subplate during fetal and early postnatal development of cat visual cortex. J Neurosci 10:2601-2613.

Fujisawa S, Amarasingham A, Harrison MT, Buzsaki G (2008) Behavior-dependent short-term assembly dynamics in the medial prefrontal cortex. Nat Neurosci 11:823-833.

Fukata Y, Adesnik H, Iwanaga T, Bredt DS, Nicoll RA, Fukata M (2006) Epilepsy-related ligand/receptor complex LGI1 and ADAM22 regulate synaptic transmission. Science 313:1792-1795.

Fukuda T (2007) Structural organization of the gap junction network in the cerebral cortex. Neuroscientist 13:199-207.

Garaschuk O, Linn J, Eilers J, Konnerth A (2000) Large-scale oscillatory calcium waves in the immature cortex. Nat Neurosci 3:452-459.

Ghosh A, Carnahan J, Greenberg ME (1994) Requirement for Bdnf in Activity-Dependent Survival of Cortical-Neurons. Science 263:1618-1623.

Gireesh ED, Plenz D (2008) Neuronal avalanches organize as nested theta- and beta/gamma-oscillations during development of cortical layer 2/3. Proc Natl Acad Sci U S A 105:7576-7581.

Golbs A, Heck N, Luhmann HJ (2007) A new technique for real-time analysis of caspase-3 dependent neuronal cell death. J Neurosci Methods 161:234-243.

Gray CM, Engel AK, Konig P, Singer W (1992) Synchronization of Oscillatory Neuronal Responses in Cat Striate Cortex - Temporal Properties. Visual Neuroscience 8:337-347.

Habets AMMC, van Dongen AMJ, van Huizen F, Corner MA (1987) Spontaneous neuronal firing patterns in fetal rat cortical networks during development in vitro: a quantitative analysis. Exp Brain Res 69:43-52.

Hanganu IL, Ben-Ari Y, Khazipov R (2006) Retinal waves trigger spindle bursts in the neonatal rat visual cortex. J Neurosci 26:6728-6736.

Hanganu IL, Kilb W, Luhmann HJ (2002) Functional synaptic projections onto subplate neurons in neonatal rat somatosensory cortex. J Neurosci 22:7165-7176.

Hanganu IL, Staiger JF, Ben-Ari Y, Khazipov R (2007) Cholinergic modulation of spindle bursts in the neonatal rat visual cortex in vivo. J Neurosci 27:5694-5705.

Hara MR, Snyder SH (2007) Cell signaling and neuronal death. Annu Rev Pharmacol Toxicol 47:117-141.

Harris KD (2005) Neural signatures of cell assembly organization. Nat Rev Neurosci 6:399-407.

Hartmann M, Heumann R, Lessmann V (2001) Synaptic secretion of BDNF after high-frequency stimulation of glutamatergic synapses. EMBO J 20:5887-5897.

Hebb DO (1949) The organization of behavior. New York: Wiley.

Heck N, Golbs A, Riedemann T, Sun JJ, Lessmann V, Luhmann HJ (2008) Activity-dependent regulation of neuronal apoptosis in neonatal mouse cerebral cortex. Cereb Cortex 18:1335-1349.

Higashi S, Molnár Z, Kurotani T, Toyama K (2002) Prenatal development of neural excitation in rat thalamocortical projections studied by optical recording. Neuroscience 115:1231-1246.

Huang EJ, Reichardt LF (2001) Neurotrophins: Roles in neuronal development and function. Annu Rev Neurosci 24:677-736.

Huberman AD, Feller MB, Chapman B (2008) Mechanisms underlying development of visual maps and receptive fields. Annu Rev Neurosci 31:479-509.

Huberman AD, Speer CM, Chapman B (2006) Spontaneous retinal activity mediates development of ocular dominance columns and binocular receptive fields in v1. Neuron 52:247-254.

Ikegaya Y, Aaron G, Cossart R, Aronov D, Lampl I, Ferster D, Yuste R (2004) Synfire chains and cortical songs: temporal modules of cortical activity. Science 304:559-564.

Kamioka H, Maeda E, Jimbo Y, Robinson HP, Kawana A (1996) Spontaneous periodic synchronized bursting during formation of mature patterns of connections in cortical cultures. Neurosci Lett 206:109-112.

Kandler K, Katz LC (1998) Coordination of neuronal activity in developing visual cortex by gap junction-mediated biochemical communication. J Neurosci 18:1419-1427.

Kanold PO (2004) Transient microcircuits formed by subplate neurons and their role in functional development of thalamocortical connections. Neuroreport 15:2149-2153.

Katz LC, Crowley JC (2002) Development of cortical circuits: Lessons from ocular dominance columns. Nat Rev Neurosci 3:34-42.

Khazipov R, Luhmann HJ (2006) Early patterns of electrical activity in the developing cerebral cortex of human and rodents. Trends in Neurosciences 29:414-418.

Khazipov R, Sirota A, Leinekugel X, Holmes GL, Ben-Ari Y, Buzsáki G (2004) Early motor activity drives spindle bursts in the developing somatosensory cortex. Nature 432:758-761.

Kilb W, Luhmann HJ (2003) Carbachol-induced network oscillations in the intact cerebral cortex of the newborn rat. Cereb Cortex 13:409-421.

Kolarow R, Brigadski T, Lessmann V (2007) Postsynaptic secretion of BDNF and NT-3 from hippocampal neurons depends on calcium calmodulin kinase II signaling and proceeds via delayed fusion pore opening. J Neurosci 27:10350-10364.

Komuro H, Kumada T (2005) Ca2+ transients control CNS neuronal migration. Cell Calcium 37:387-393.

Kriegstein AR, Noctor SC (2004) Patterns of neuronal migration in the embryonic cortex. Trends Neurosci 27:392-399.

Kuczewski N, Porcher C, Ferrand N, Fiorentino H, Pellegrino C, Kolarow R, Lessmann V, Medina I, Gaiarsa JL (2008) Backpropagating action potentials trigger dendritic release of BDNF during spontaneous network activity. J Neurosci 28:7013-7023.

Lapray D (2009) Stimulus-induced gamma activity in the electrocorticogram of freely moving telemetric implanted rats: the neuronal signature of novelty detection. PhD dissertation.

Le Van QM, Khalilov I, Ben-Ari Y (2006) The dark side of high-frequency oscillations in the developing brain. Trends Neurosci 29:419-427.

Lee LJ, Iwasato T, Itohara S, Erzurumlu RS (2005) Exuberant thalamocortical axon arborization in cortex-specific NMDAR1 knockout mice. J Comp Neurol 485:280-292.

Lessmann V, Gottmann K, Malcangio M (2003) Neurotrophin secretion: current facts and future prospects. Prog Neurobiol 69:341-374.

Lewicki MS (1998) A review of methods for spike sorting: the detection and classification of neural action potentials. Network 9:R53-R78.

Liu X, Wang Q, Haydar TF, Bordey A (2005) Nonsynaptic GABA signaling in postnatal subventricular zone controls proliferation of GFAP-expressing progenitors. Nat Neurosci 8:1179-1187.

Llinas RR (1988) The Intrinsic Electrophysiological Properties of Mammalian Neurons - Insights Into Central Nervous-System Function. Science 242:1654-1664.

Lohmann C, Wong RO (2005) Regulation of dendritic growth and plasticity by local and global calcium dynamics. Cell Calcium 37:403-409.

LoTurco JJ, Kriegstein AR (1991) Clusters of coupled neuroblasts in embryonic neocortex. Science 252:563-566.

MacLean JN, Watson BO, Aaron GB, Yuste R (2005) Internal dynamics determine the cortical response to thalamic stimulation. Neuron 48:811-823.

Madhavan R, Chao ZC, Potter SM (2007) Plasticity of recurring spatiotemporal activity patterns in cortical networks. Phys Biol 4:181-193.

Mao BQ, Hamzei-Sichani F, Aronov D, Froemke RC, Yuste R (2001) Dynamics of spontaneous activity in neocortical slices. Neuron 32:883-898.

Markram H, Toledo-Rodriguez M, Wang Y, Gupta A, Silberberg G, Wu CZ (2004) Interneurons of the neocortical inhibitory system. Nat Rev Neurosci 5:793-807.

Marom S, Shahaf G (2002) Development, learning and memory in large random networks of cortical neurons: lessons beyond anatomy. Quarterly Reviews of Biophysics 35:63-87.

Marshall CA, Suzuki SO, Goldman JE (2003a) Gliogenic and neurogenic progenitors of the subventricular zone: who are they, where did they come from, and where are they going? Glia 43:52-61.

Marshall J, Dolan BM, Garcia EP, Sathe S, Tang XL, Mao ZX, Blair LAC (2003b) Calcium channel and NMDA receptor activities differentially regulate nuclear C/EBP beta levels to control neuronal survival. Neuron 39:625-639.

McCabe AK, Chisholm SL, Picken-Bahrey HL, Moody WJ (2006) The self-regulating nature of spontaneous synchronized activity in developing mouse cortical neurones. J Physiol 577:155-167.

Mechawar N, Descarries L (2001) The cholinergic innervation develops early and rapidly in the rat cerebral cortex: A quantitative immunocytochemical study. Neuroscience 108:555-567.

Milh M, Kaminska A, Huon C, Lapillonne A, Ben-Ari Y, Khazipov R (2007) Rapid cortical oscillations and early motor activity in premature human neonate. Cereb Cortex 17:1582-1594.

Minlebaev M, Ben-Ari Y, Khazipov R (2007) Network mechanisms of spindle-burst oscillations in the neonatal rat barrel cortex in vivo. J Neurophysiol 97:692-700.

Molnar Z, Kurotani T, Higashi S, Yamamoto N, Toyama K (2003) Development of functional thalamocortical synapses studied with current source-density analysis in whole forebrain slices in the rat. Brain Research Bulletin 60:355-371.

Moody WJ, Bosma MM (2005) Ion channel development, spontaneous activity, and activity-dependent development in nerve and muscle cells. Physiol Rev 85:883-941.

Morgan RJ, Soltesz I (2008) Nonrandom connectivity of the epileptic dentate gyrus predicts a major role for neuronal hubs in seizures. Proc Natl Acad Sci U S A 105:6179-6184.

Nadasdy Z (2000) Spike sequences and their consequences. Journal of Physiology-Paris 94:505-524.

Nadasdy Z, Hirase H, Czurko A, Csicsvari J, Buzsaki G (1999) Replay and time compression of recurring spike sequences in the hippocampus. J Neurosci 19:9497-9507.

Nicol X, Voyatzis S, Muzerelle A, Narboux-Neme N, Südhof TC, Miles R, Gaspar P (2007) cAMP oscillations and retinal activity are permissive for ephrin signaling during the establishment of the retinotopic map. Nat Neurosci 10:340-347.

Nicolelis MAL, Fanselow EE, Ghazanfar AA (1997a) Hebb's dream: The resurgence of cell assemblies. Neuron 19:219-221.

Nicolelis MAL, Ghazanfar AA, Faggin BM, Votaw S, Oliveira LMO (1997b) Reconstructing the engram: Simultaneous, multisite, many single neuron recordings. Neuron 18:529-537.

Noctor SC, Flint AC, Weissman TA, Dammerman RS, Kriegstein AR (2001) Neurons derived from radial glial cells establish radial units in neocortex. Nature 409:714-720.

Opitz T, De Lima AD, Voigt T (2002) Spontaneous development of synchronous oscillatory activity during maturation of cortical networks in vitro. J Neurophysiol 88:2196-2206.

Pasquale V, Massobrio P, Bologna LL, Chiappalone M, Martinoia S (2008) Self-organization and neuronal avalanches in networks of dissociated cortical neurons. Neuroscience 153:1354-1369.

Pastalkova E, Itskov V, Amarasingham A, Buzsaki G (2008) Internally generated cell assembly sequences in the rat hippocampus. Science 321:1322-1327.

Peinado A (2000) Traveling slow waves of neural activity: A novel form of network activity in developing neocortex. J Neurosci 20:NIL1-NIL6.

Plenz D, Thiagarajan TC (2007) The organizing principles of neuronal avalanches: cell assemblies in the cortex? Trends in Neurosciences 30:101-110.

Potter SM, DeMarse TB (2001) A new approach to neural cell culture for long-term studies. J Neurosci Methods 110:17-24.

Purves D, AUGUSTINE GJ, Fitzparick D, LaMANTIA A, McNAMARA JO, William SM (2001) Neuroscience, 2nd edition. Sinauer Associates, Inc.

Raichman N, Ben Jacob E (2008) Identifying repeating motifs in the activation of synchronized bursts in cultured neuronal networks. J Neurosci Methods 170:96-110.

Rakic P (1972) Extrinsic cytological determinants of basket and stellate cell dendritic pattern in the cerebellar molecular layer. J Comp Neurol 146:335-354.

Rakic P (1988) Specification of cerebral cortical areas. Science 241:170-176.

Redmond L, Ghosh A (2005) Regulation of dendritic development by calcium signaling. Cell Calcium 37:411-416.

Ritz R, Sejnowski TJ (1997) Synchronous oscillatory activity in sensory systems: new vistas on mechanisms. Curr Opin Neurobiol 7:536-546.

Rolston JD, Wagenaar DA, Potter SM (2007) Precisely timed spatiotemporal patterns of neural activity in dissociated cortical cultures. Neuroscience 148:294-303.

Roskies AL (1999) The binding problem - Introduction. Neuron 24:7-+.

Sanchez-Vives MV, McCormick DA (2000) Cellular and network mechanisms of rhythmic recurrent activity in neocortex. Nat Neurosci 3:1027-1034.

Schmitz D, Schuchmann S, Fisahn A, Draguhn A, Buhl EH, Petrasch-Parwez E, Dermietzel R, Heinemann U, Traub RD (2001) Axo-axonal coupling: a novel mechanism for ultrafast neuronal communication. Neuron 31:831-840.

Schrader S, Grun S, Diesmann M, Gerstein GL (2008) Detecting synfire chain activity using massively parallel spike train recording. J Neurophysiol 100:2165-2176.

Segev R, Baruchi I, Hulata E, Ben-Jacob E (2004) Hidden neuronal correlations in cultured networks. Phys Rev Lett 92:118102.

Sejnowski TJ, Destexhe A (2000) Why do we sleep? Brain Res 886:208-223.

Spitzer NC (2002) Activity-dependent neuronal differentiation prior to synapse formation: the functions of calcium transients. J Physiol Paris 96:73-80.

Spitzer NC (2006) Electrical activity in early neuronal development. Nature 444:707-712.

Spitzer NC, Root CM, Borodinsky LN (2004) Orchestrating neuronal differentiation: patterns of Ca2+ spikes specify transmitter choice. Trends Neurosci 27:415-421.

Stoppini L, Buchs PA, Muller D (1991) A simple method for organotypic cultures of nervous tissue. J Neurosci Methods 37:173-182.

Sun JJ, Kilb W, Luhmann HJ (2009) Self-organization of recurrent spike patterns in developing neuronal networks *in-vitro*. In preparation.

Sun JJ, Luhmann HJ (2007) Spatio-temporal dynamics of oscillatory network activity in the neonatal mouse cerebral cortex. Eur J Neurosci 26:1995-2004.

Torborg CL, Feller MB (2005) Spontaneous patterned retinal activity and the refinement of retinal projections. Prog Neurobiol 76:213-235.

Torrence C, Compo GP (1998) A practical guide to wavelet analysis. Bull Am Meterol Soc 79:61-78.

Tseng KY, O'Donnell P (2005) Post-pubertal emergence of prefrontal cortical up states induced by D1-NMDA co-activation. Cereb Cortex 15:49-57.

van Pelt J, Corner MA, Wolters PS, Rutten WL, Ramakers GJ (2004) Longterm stability and developmental changes in spontaneous network burst firing patterns in dissociated rat cerebral cortex cell cultures on multielectrode arrays. Neurosci Lett 361:86-89.

Vanhatalo S, Palva JM, Andersson S, Rivera C, Voipio J, Kaila K (2005) Slow endogenous activity transients and developmental expression of K+-Cl- cotransporter 2 in the immature human cortex. Eur J Neurosci 22:2799-2804.

Varela F, Lachaux JP, Rodriguez E, Martinerie J (2001) The brainweb: Phase synchronization and large-scale integration. Nat Rev Neurosci 2:229-239.

Wagenaar DA, Madhavan R, Pine J, Potter SM (2005) Controlling bursting in cortical cultures with closed-loop multi-electrode stimulation. J Neurosci 25:680-688.

Wagenaar DA, Pine J, Potter SM (2006) An extremely rich repertoire of bursting patterns during the development of cortical cultures. BMC Neurosci 7:11.

Wagner J, Luhmann HJ (2006) Activation of metabotropic glutamate receptors induces propagating network oscillations in the intact cerebral cortex of the newborn mouse. Neuropharmacology 51:848-857.

Wehr M, Laurent G (1996) Odour encoding by temporal sequences of firing in oscillating neural assemblies. Nature 384:162-166.

Weissman TA, Riquelme PA, Ivic L, Flint AC, Kriegstein AR (2004) Calcium waves propagate through radial glial cells and modulate proliferation in the developing neocortex. Neuron 43:647-661.

Williams K (1993) Ifenprodil discriminates subtypes of the N-methyl-D-aspartate receptor: selectivity and mechanisms at recombinant heteromeric receptors. Mol Pharmacol 44:851-859.

Windhorst U, Johansson H (1999) Modern techniques in neuroscience research. Springer-Verlag.

Wonders CP, Anderson SA (2006) The origin and specification of cortical interneurons. Nat Rev Neurosci 7:687-696.

Woolsey TA, Van der Loos H (1970) The structural organization of layer IV in the somatosensory region (SI) of mouse cerebral cortex. The description of a cortical field composed of discrete cytoarchitectonic units. Brain Res 17:205-242.

Wu C, Asl MN, Gillis J, Skinner FK, Zhang L (2005a) An in vitro model of hippocampal sharp waves: regional initiation and intracellular correlates. J Neurophysiol 94:741-753.

Wu C, Luk WP, Gillis J, Skinner F, Zhang L (2005b) Size does matter: generation of intrinsic network rhythms in thick mouse hippocampal slices. J Neurophysiol 93:2302-2317.

Yuste R, Nelson DA, Rubin WW, Katz LC (1995) Neuronal domains in developing neocortex: Mechanisms of coactivation. Neuron 14:7-17.

Yuste R, Peinado A, Katz LC (1992) Neuronal domains in developing neocortex. Science 257:665-669.

Zhang LI, Tao HW, Holt CE, Harris WA, Poo MM (1998) A critical window for cooperation and competition among developing retinotectal synapses. Nature 395:37-44.

Acknowledgments

Thanks to my supervisor, for giving me the opportunity to work in his lab.

Thanks to the members of my jury.

Thanks to those who helped me on this manuscript.

Thanks to all students and members of the lab, helping me so much, it has been a lot of fun studying in Germany.

Curriculum vitae

Jyh-Jang SUN

Institute of Physiology and Pathophysiology

Johannes Gutenberg-University Mainz

Duesbergweg 6, D-55128 Mainz, Germany

Tel.: +49 (06131) 39-25648

Fax: +49 (06131) 39-26071

E-mail: sunj@uni-mainz.de

Date of Birth: 11.April.1974.

Place of Birth: Jang-Hua County, Taiwan

Nationality: Taiwan

Education

4/2005-	**PhD student in Neurophysiology** under Prof. Dr. Heiko J. Luhmann, Johannes Gutenberg-University Mainz, Germany
	Member of the Neuroscience Graduate Program (DFG GRK), Johannes Gutenberg-University Mainz, Germany
8/2000 – 3/2005	**Research Assistant for Neuroscience** as a military duty in Dr. Shyu Bai-Chung's Lab, Institute of Biomedical Sciences, Academia Sinica, Taiwan
9/1998 – 7/2000	**MSc. in Neuroscience** under Prof. Dr. Chang Yen-Chung, Institute of life sciences, National Tsing-Hua University, Taiwan
9/1993 – 7/1998	BA, Department of **Veterinary Medicine**, National Chung-Hsing University**,** Taiwan

Publications

Sun, J.J, Kilb W., Luhmann, H.J. (2009)

Self-organization of recurrent spike patterns in developing neuronal networks *in vitro*.

In preparation.

Yang, J.W., Hanganu-Opatz, I.L., **Sun**, J.J., Luhmann, H.J. (2009)
Three patterns of oscillatory activity differentially synchronize developing neocortical networks *in vivo.*

J. Neuroscience accepted.

Heck, N., Golbs, A., Riedemann, T., **Sun**, J.J., Lessmann, V. & Luhmann, H.J. (2008)
Activity-dependent regulation of neuronal apoptosis in neonatal mouse cerebral cortex.
Cerebral Cortex 18(6):1335-49.

Sun, J.J. & Luhmann, H.J. (2007)
Spatio-temporal dynamics of oscillatory network activity in the neonatal mouse cerebral cortex.
Eur. J. Neuroscience 26(7):1995-2004.

Sun J.J., Yang J.W., Shyu B.C. (2006)

Current source density analysis of laser heat-evoked intra-cortical field potentials in the primary somatosensory cortex of rats.

Neuroscience 140(4):1321-36.

Sun J.J., Chuang Kung J., Wang C.C., Chen S.L., Shyu B.C. (2006)

Short-term facilitation in the anterior cingulate cortex following stimulation of the medial thalamus in the rat.

Brain Res. 1097(1):101-15.

Wang Z.H., Chang M.H., Yang J.W., **Sun** J.J., Lee H.C., Shyu B.C. (2006)

Layer IV of the primary somatosensory cortex has the highest complexity under anesthesia and cortical complexity is modulated by specific thalamic inputs.

Brain Res. 1082(1):102-14.

Shyu B.C., Lin C.Y., **Sun** J.J., Sylantyev S., Chang C. (2004)

A method for direct thalamic stimulation in fMRI studies using a glass-coated carbon fiber electrode.

J Neurosci Methods 137(1):123-31.

Shyu B.C., Lin C.Y., **Sun** J.J., Chen S.L., Chang C. (2004)

BOLD response to direct thalamic stimulation reveals a functional connection between the medial thalamus and the anterior cingulate cortex in the rat.

Magn Reson Med. 52(1):47-55.

Poster presentations

Sun J.J., Kilb W. & Luhmann H.J.

Activity-dependent self-organization of neuronal networks in culture on micro-electrode array (MEA).

6th FENS meeting, 2008, Geneva, Switzerland.

Yang J.W., Hanganu I.L., **Sun** J.J. & Luhmann H. J.

Synchronization pattern of oscillatory activity in the neonatal rat somatosensory cortex *in vivo*.

6th FENS meeting, 2008, Geneva, Switzerland.

Golbs A., Heck N., **Sun** J.J. & Luhmann H.J.

Influence of different activity patterns on the survival of immature cortical neurons under trophic deprivation.

6th FENS meeting, 2008, Geneva, Switzerland.

Sun J.J. & Luhmann H.J.

Oscillatory network activity in the newborn mouse cerebral cortex studied with MEA.

5th FENS meeting, 2006, Vienna, Austria.

Sun J.J. & Luhmann H.J.

Spatio-temporal dynamics of oscillatory network activity in the neonatal mouse cerebral cortex.

MEA meeting, 2006, Reutlingen, Germany.

Sun J.J., Chen T.C., Shyu B.C.

Electrophysiological and morphological properties of neurons in the rat primary somatosensory cortex response to short CO_2 laser pulses: An *in vivo* intracellular recording study.

Society for Neuroscience annual meeting, 2004, San Diego, USA.

Sun J.J., Yang J.W., Chen T.C. and Shyu B.C.

Cortical circuitry of thermal nociception in the primary somatosensory cortex of rats.

4th FENS meeting, Lisbon, 2004.

Sun, J.J., Yang J.W., Chang M.H., Chou P.H., Shyu B.C.

The current source density analysis of laser evoked potentials using multichannel recordings in the somatosensory cortex of rats.

Society for Neuroscience annual meeting, 2003, New Orleans, USA.

Shyu B.C., **Sun** J.J., Chang M.H., Lee C.M.

The current source density analysis of the paired-pulse facilitation of the field potentials in the anterior cingulate cortex *in vivo*.

6th IBRO World Congress of Neuroscience, 2003, Prague, Czech.

Sun J.J., Chang M.H., Chai S.C., Shyu B.C.

The current source density analysis of the paired-pulse facilitation in the anterior cingulate cortex *in vivo*.

19th Annual Conference of the Taiwan Society for Biochemistry and Molecular Biology, 2003, Taipei, Taiwan

Chang M.H., **Sun** J.J., Wang Z.H., Shyu B.C.

Application of nonlinear time series analysis on multichannel EEG in rats under halothane anesthesia.

The Annual Meeting of the Chinese Pain Society, 2003, Taipei, Taiwan.

Sun J.J., Cheng S.Y., Chen S.L., Chai S.C., Shyu B.C.

The Influence of peripheral stimulation on the paired-pulse facilitation in the anterior cingulate cortex of the rat.

Society for Neuroscience annual meeting, 2002, Orlando, USA.

Chen W.F., **Sun** J.J., Chen Y.J., Shyu B.C.

Electrophysiological study of the nociceptive responses in the anterior cingulated cortex in rats.

Taiwan Society of Clinical Neurophysiology, 2002, Taipei, Taiwan.

Lin C., **Sun** J.J., Chen S.L, Chang C., Hou W., Shyu B.C.

A fMRI study of the anterior cingulate cortex activations during direct electrical stimulation of the medial thalamus in rats.

10th World Congress on Pain, 2002, San Diego, USA.

Sun J.J., Cheng S.Y., Chen S.L., Wang C.C. and Shyu B.C.

Field potentials and multiple unit activities mapping of the paired-pulse facilitation in the anterior cingulate cortex of the rat following stimulation in the medial thalamus.

Taiwan Society of Clinical Neurophysiology, 2001, Taipei, Taiwan.

Courses

Aug 2008: Lectures of "**Theoretical neuroscience and complex system**", FIAS, Johann Wolfgang Goethe University, Frankfurt am Main, Germany.

October 2006: BCCN/NWG course on "**Analysis and Models in Neurophysiology**", Institute of Biology, Albert-Ludwigs University, Freiburg, Germany.

Appendix

Matlab codes

Time-frequency colormap by wavelet

Filename: `J_wavelet.m`

```
function [ccfs,bound] = J_wavelet(wavelet_data,Fs,FFTMax)
%2009 copyright reserved to Jyh-Jang Sun, Jenq-Wei Yang and
%Prof. Luhmann, Mainz University, Germany
%Any modification on this function, please inform me via
%sunj@uni-mainz.de
%If you use this function please cite the resource:
%Sun, J.J. & Luhmann, H.J. (2007)
%Spatio-temporal dynamics of oscillatory network activity in
%the neonatal mouse cerebral cortex.
%Eur. J. Neuroscience, 26(7):1995-2004.

wname = 'morl';%wavelet form
delta = 1/Fs;%sampling period
cfreq = centfrq(wname,8);%center frequency (Hz)
Step=0.2;%frequency resolution
Freq=[0.1:Step:FFTMax];%define the frequency

for j=1:size(Freq,2)
    ScaleW(j)=cfreq/(delta*Freq(j));%frequency to scale%%%%
End

ccfs =cwt(wavelet_data,ScaleW,wname);%wavelet02 calculation
ccfs=ccfs.^2;
ccfs=rot90(ccfs); % rot array

%smooth
ccfsS=smooth(ccfs,size(wavelet_data,2)*3/100);
ccfs=reshape(ccfsS,size(ccfs,1),size(ccfs,2));
ccfs=rot90(ccfs);
ccfs=fliplr(ccfs);
ccfs=(ccfs)/(max(max(ccfs(1:(size(ccfs,1)-5),:)))); %normalize

%significant area
nSTDs=2.58;% 99% significant level
nSTDs95=1.96;% 95% significant level
bound=mean(mean(ccfs,1))+nSTDs95/(size(ccfs,1).^(1/2));
```

Template-matching algorithm

Filename: tm.m

```
function [pn,patternMatrixOri,MaxPoint] =
tm(Template,TimeWindow,MinTemplateNumber,MaxTemplateNumber)
%2009 copyright reserved to Jyh-Jang Sun, Prof. Luhmann's %Lab,
%Mainz University, Germany
%Any modification on this tm.m, please inform me via
%sunj@uni-mainz.de
%Please cite the resource by 'Jyh-Jang Sun, %Werner Kilb and
%Heiko J. Luhmann, Self-organization of recurrent spike
%patterns in developing neuronal networks in vitro, 2009
%unpublished'

%This function is based on the algorithms of Abeles and
%Gerstein, 1988.
%Input parameters
%Template: get the raw data, containing 1st row, neuron
%indices, 2nd raw,
%spike timing
%TimeWindow: set the time window for template
%MinTemplateNumber: the minimal complexity of patterns
%MaxTemplateNumber: the maximal complexity of patterns

%output data
%pn: repetition and complexity of patterns aligned column by
%column.
%patternMatrixOri: the pattern information including 1st
%row, neuron indices, 2nd up to maximal repetition's row,
%spike times
%MaxPoint: the maximal complexity of pattern

MaxPoint=zeros(MaxTemplateNumber,1);
[Y,I]=sort(Template,2);
for i=1:size(Y,2)
    Y(2,i)=Template(2,I(1,i));
End

Y=round(Y);
[K,L]=unique(Y(1,:),'first');
k=1;
TemplateMatchM2={};

for i=1:size(L,2)
    I=find(Y(1,:)-Y(1,L(i))<=TimeWindow);
    Zu=max(I);
    YM=Y(:,L(i):Zu);
    StartTimeM(k)=YM(1,1);
    YM(1,:)=YM(1,:)-YM(1,1)+1;
    Matcha1Pic=zeros(max(Y(2,:)),TimeWindow+1)+10+k;

    for j=1:size(YM,2)
        Matcha1Pic(YM(2,j),YM(1,j))=1;
```

```
    end
    TemplateMatchM2{i}=Matcha1Pic;
    k=k+1;
end

pnInf=[0;0];
patternMatrix3DM={};
kn=0;
PatternMN={};
PattersCha=[];
LatLim=10;%set the spike-spike latency is less than LatLim %ms

for i1=1:k-2
    Matcha1Pic=TemplateMatchM2(Fukata et al., 2006);
    for i2=i1+1:k-1
        Matcha2Pic=TemplateMatchM2{i2};
        [I,J]=find(Matcha1Pic==Matcha2Pic);
        J=rot90(J);I=rot90(I);Imean=mean(I);
        DiffJ=diff(J);
        if size(I,2)>=MinTemplateNumber && max(DiffJ)<=LatLim
           && I(1)~=Imean
           kn=kn+1;
           J=J-J(1)+1;
           PatternMN{kn}=[I;J];
           PattersCha(kn)=100*sum(I)+10*sum(J);
        end
    end
end

%reduce the pattern number if the pattern is exactly the same
PatternMN2={};
[K2,L2]=unique(PattersCha);

for i5=1:size(L2,2)
    PatternMN2{i5}=PatternMN{L2(i5)};
end

%use template to search all templates
if size(L2,2)>0
   for i=1:size(L2,2)
       Matcha1=PatternMN2{i};
       Count2=0;patternMatrix3DMTemp=[];
       for j2=1:size(TemplateMatchM2,2)
               Matcha2Pic=TemplateMatchM2{j2};
               CheckM=[];
               for j3=1:size(Matcha1,2)
                   Test1=Matcha1(:,j3);
                   if Matcha2Pic(Test1(1,1),Test1(2,1))==1
                      CheckM(j3)=1;
                   end
               end
               CheckSum=sum(CheckM);
               if CheckSum==size(Matcha1,2)
                  I=Matcha1(1,:);
                  J=Matcha1(2,:);
```

```
                    Count2=Count2+1;
                    patternMatrix3DMTemp(1,1:size(J,2))=[I];

                    patternMatrix3DMTemp(Count2+1,1:size(J,2))=
                    [J+StartTimeM(j2)-1];

                    pnInf(:,i)=[Count2;size(I,2)];%1,repeat

                    %times and 2, point
                    if MaxPoint(size(I,2),1)<Count2;
                       MaxPoint(size(I,2),1)=Count2;
                    end
                end
        end
        patternMatrix3DM{i}=patternMatrix3DMTemp;
    end
end


patternMatrixOri=patternMatrix3DM;
pn=pnInf;
```

Auto- cross-correlation in spikes

Filename: J_crosscorr.m

```
function [XCF,Lags] =
J_crosscorr(spiketimesX,spiketimesY,nLags)
%2009 copyright reserved to Jyh-Jang Sun, Prof. Luhmann's Lab,
%Mainz University, Germany
%Any modification on J_crosscorr.m, please inform me via
%sunj@uni-mainz.de
%Please cite the resource by 'Jyh-Jang Sun, %Werner Kilb and
%Heiko J. Luhmann, Self-organization of %recurrent spike
%patterns in developing neuronal networks in %vitro, 2009
%unpublished'

%purpose-this function is for the calculation of auto- %cross-
%correlation between spike data with values of 0 and 1.

%Input parameters
%spiketimesX-1st vector of observations has values of 0 or 1
%spiketimesY-2nd vector of observations has values of 0 or 1
%nLags-Positive, scalar integer indicating the number of lags
%of the XCF to compute.

%output data
%XCF-XCF is a vector of length 2*nLags + 1 corresponding to
%lags 0, +/-1, +/-2,... +/-nLags.
%Lags-Vector of lags corresponding to XCF (-nLags to %+nLags).

for k=-nLags:nLags
    count=0;
    spiketimesA=spiketimesX+k;
    for m=1:length(spiketimesY)
        K=find(spiketimesA-spiketimesY(m)==0);
        N=length(K);
        count=count+N;
    end

    XCFJ((nLags+k)+1)=count;
end
Lags=-nLags:nLags;
XCF=XCFJ/size(spiketimesX,1);
```